nature medicine

Nogo-B regulates endothelial sphingolipid homeostasis to control vascular function and blood pressure

Anna Cantalupo[1,6], Yi Zhang[1,6], Milankumar Kothiya[1], Sylvain Galvani[1], Hideru Obinata[1], Mariarosaria Bucci[2], Frank J Giordano[3,4], Xian-Cheng Jiang[5], Timothy Hla[1] & Annarita Di Lorenzo[1]

Endothelial dysfunction is a critical factor in many cardiovascular diseases, including hypertension. Although lipid signaling has been implicated in endothelial dysfunction and cardiovascular disease, specific molecular mechanisms are poorly understood. Here we report that Nogo-B, a membrane protein of the endoplasmic reticulum, regulates endothelial sphingolipid biosynthesis with direct effects on vascular function and blood pressure. Nogo-B inhibits serine palmitoyltransferase, the rate-limiting enzyme of the *de novo* sphingolipid biosynthetic pathway, thereby controlling production of endothelial sphingosine 1-phosphate and autocrine, G protein–coupled receptor–dependent signaling by this metabolite. Mice lacking Nogo-B either systemically or specifically in endothelial cells are hypotensive, resistant to angiotensin II–induced hypertension and have preserved endothelial function and nitric oxide release. In mice that lack Nogo-B, pharmacological inhibition of serine palmitoyltransferase with myriocin reinstates endothelial dysfunction and angiotensin II–induced hypertension. Our study identifies Nogo-B as a key inhibitor of local sphingolipid synthesis and shows that autocrine sphingolipid signaling within the endothelium is critical for vascular function and blood pressure homeostasis.

© 2015 Nature America, Inc. All rights reserved.

Nearly 1 billion people worldwide are affected by hypertension. Despite current pharmacological approaches to control blood pressure, this condition remains one of the most common causes of heart failure, kidney disease and stroke[1]. Endothelial dysfunction is associated with hypertension, and is an early event contributing to vascular tone dysregulation[2–4].

Endothelium-released nitric oxide (NO) is of critical importance for the maintenance of normal blood pressure[5–7]. Sphingolipids, particularly sphingosine-1-phosphate (S1P), have emerged as a class of bioactive lipids with important functions in cardiovascular homeostasis, including blood pressure control. Acting through G protein–coupled S1P receptors, S1P regulates arterial tone. At low concentrations, S1P induces vasodilation through the receptors $S1P_1$ and $S1P_3$ on endothelial cells, via activation of endothelial nitric oxide synthase (eNOS) and NO[8,9]. At higher concentrations, S1P causes vasoconstriction through $S1P_2$ and $S1P_3$ activation on vascular smooth muscle cells (VSMCs)[10,11].

The endothelium is not only a target of S1P action but also an important source of plasma S1P[12]; red blood cells are the major source[12–14]. Stimulated by blood flow, endothelial-derived S1P is transported out of the cell through the spinster-2 transporter[15]; S1P activates $S1P_1$ on the cell surface in an autocrine fashion to induce barrier-protective effects[16] and control vascular tone. Moreover, a recent study reported that $S1P_1$ is required for eNOS-activation in response to shear stress[17]. These findings suggest that S1P levels within the vascular wall must be tightly controlled to maintain vascular homeostasis. How S1P production within the vascular wall is regulated and the roles of S1P in physiological and hypertensive conditions are still unknown.

Sphingolipids are produced by the *de novo* biosynthetic pathway in the endoplasmic reticulum (ER). The rate-limiting enzyme, serine palmitoyltransferase (SPT), catalyzes the condensation of serine and palmitoyl-coenzyme A[18,19]. Because sphingolipids are involved in many pathophysiological processes, the expression and regulation of SPT has attracted much attention. A recently discovered major regulatory system for SPT involves ORMDL proteins[20,21], which have been suggested to be involved in childhood asthma on the basis of genome-wide association studies[22]. Here we identify Nogo-B, a membrane protein of the ER and part of the reticulon-4 (Rtn4) protein family, as a key negative regulator of *de novo* sphingolipid biosynthesis and reveal the importance of local sphingolipid homeostasis in preserving endothelial function and blood pressure.

RESULTS

Nogo-B regulates blood pressure through an eNOS pathway

Nogo-B belongs to the Rtn4 family of proteins, which comprises three major splice isoforms: Nogo-A and Nogo-C are abundantly expressed in the central nervous system, and Nogo-C[23,24] is also found in skeletal muscle; Nogo-B is expressed highly but not exclusively in endothelial cells and VSMCs of blood vessels, including mesenteric arteries[25] (**Fig. 1a**). Mice lacking the Nogo-A and Nogo-B isoforms (hereafter referred to as Nogo-A/B-deficient mice)[24], were markedly

[1]Center for Vascular Biology, Department of Pathology and Laboratory Medicine, Weill Cornell Medical College, Cornell University, New York, New York, USA. [2]Department of Pharmacy, University of Naples "Federico II", Naples, Italy. [3]Section of Cardiovascular Medicine, Department of Internal Medicine, Yale University School of Medicine, New Haven, Connecticut, USA. [4]Vascular Biology and Therapeutic Program, Yale University School of Medicine, New Haven, Connecticut, USA. [5]Department of Anatomy and Cell Biology, State University of New York, Downstate Medical Center, Brooklyn, New York, USA. [6]These authors contributed equally to this work. Correspondence should be addressed to A.D.L. (and2039@med.cornell.edu).

Received 1 April; accepted 27 July; published online 24 August 2015; doi:10.1038/nm.3934

hypotensive compared to wild-type (WT) control mice (**Fig. 1b**), with no significant increase in heart rate. Consistent with their lower blood pressure, the thickness/radius ratio of the mesenteric arteries of Nogo-A/B-deficient mice was significantly reduced as compared with WT mice (**Fig. 1b**). To assess the role of Nogo-B in VSMC function, we evaluated vasoconstriction in the mesenteric arteries of WT and Nogo-A/B-deficient mice in response to increasing concentrations of the adrenergic α_1 receptor agonist phenylephrine (PE), the thromboxane A_2 receptor agonist U-46619 and S1P ($S1P_2$ and $S1P_3$ receptor ligand). We found no differences between the two groups of mice in the vasoconstrictive responses of the mesenteric arteries (**Supplementary Fig. 1a–c** and **Supplementary Data 1**), suggesting that hypotension in Nogo-A/B-deficient mice cannot be ascribed to an impaired contractility of resistance vessels. Accordingly, we focused on the role of Nogo-B in the endothelium.

Given the important role of NO as an endogenous endothelial-derived vasodilator, we assessed the activation of eNOS. Nogo-A/B-deficient aortas showed a marked increase of eNOS phosphorylated at Ser1176 (p-Ser1176-eNOS) as compared to WT aortas, as assessed by western blot and *en face* immunofluorescence staining (**Fig. 1c**,**d**), whereas total eNOS (**Fig. 1c** and **Supplementary Fig. 1d**) and neuronal NOS (nNOS) (**Supplementary Fig. 1e**) levels were unchanged.

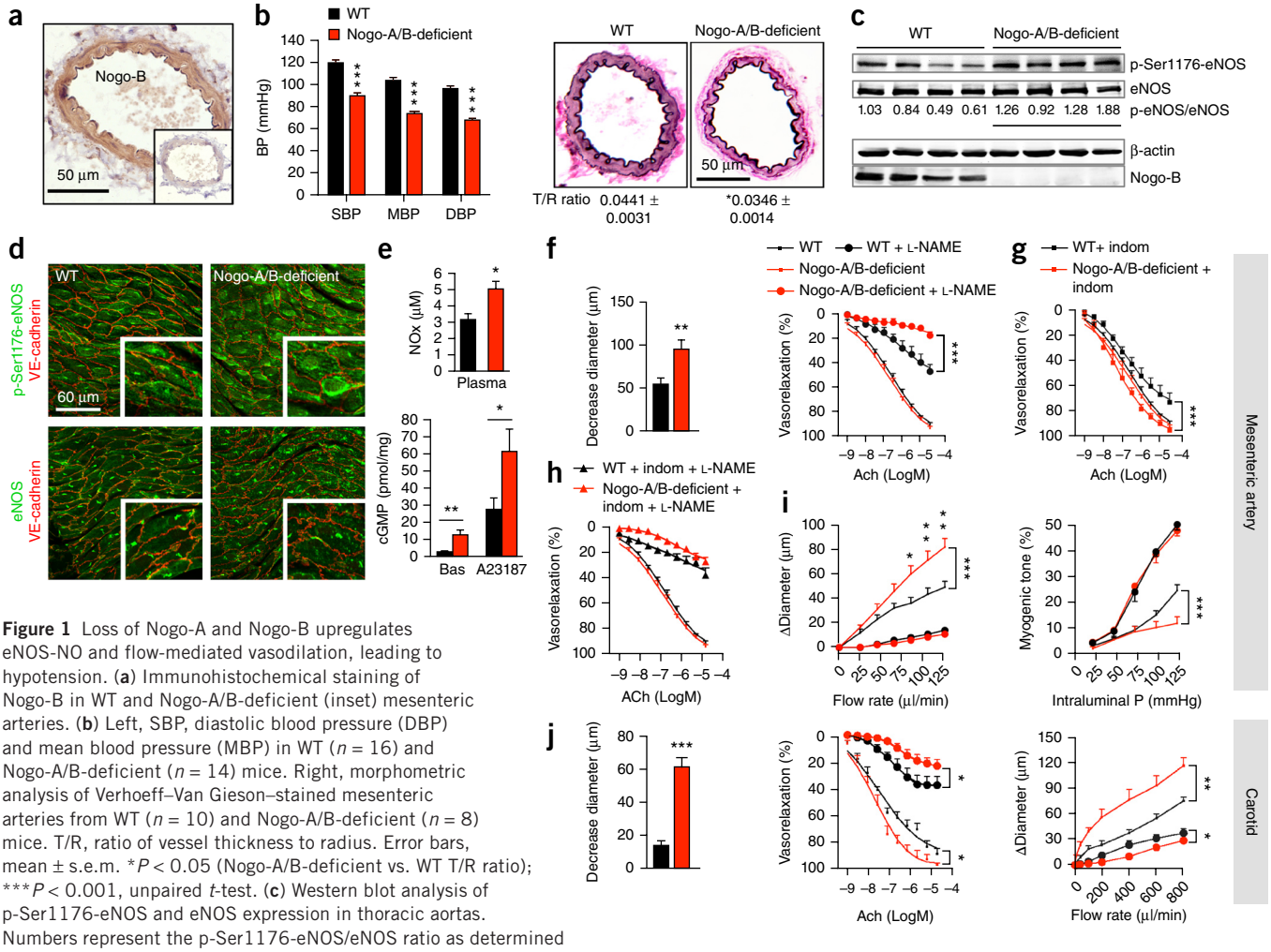

Figure 1 Loss of Nogo-A and Nogo-B upregulates eNOS-NO and flow-mediated vasodilation, leading to hypotension. (**a**) Immunohistochemical staining of Nogo-B in WT and Nogo-A/B-deficient (inset) mesenteric arteries. (**b**) Left, SBP, diastolic blood pressure (DBP) and mean blood pressure (MBP) in WT ($n = 16$) and Nogo-A/B-deficient ($n = 14$) mice. Right, morphometric analysis of Verhoeff–Van Gieson–stained mesenteric arteries from WT ($n = 10$) and Nogo-A/B-deficient ($n = 8$) mice. T/R, ratio of vessel thickness to radius. Error bars, mean ± s.e.m. $^*P < 0.05$ (Nogo-A/B-deficient vs. WT T/R ratio); $^{***}P < 0.001$, unpaired *t*-test. (**c**) Western blot analysis of p-Ser1176-eNOS and eNOS expression in thoracic aortas. Numbers represent the p-Ser1176-eNOS/eNOS ratio as determined by densitometric analysis. β-actin was used as a loading control. (**d**) *En face* staining of WT and Nogo-A/B-deficient aortas for eNOS, p-Ser1176-eNOS and vascular endothelial (VE)-cadherin. (**e**) Top, plasma levels of nitrite (NOx) in WT and Nogo-A/B-deficient mice ($n = 9$ mice per group); bottom, basal (Bas) and A23187-stimulated cGMP concentrations in aortas from WT and Nogo-A/B-deficient mice ($n = 5$ mice per group). Error bars, mean ± s.e.m. $^*P < 0.05$; $^{**}P < 0.01$, unpaired *t*-test (top) or one-way ANOVA (bottom). (**f**) Left, L-NAME–induced decrease in luminal diameter versus baseline in mesenteric arteries from WT ($n = 9$) and Nogo-A/B-deficient ($n = 7$) mice. Right, Ach concentration-response curves with or without L-NAME treatment in mesenteric arteries from WT ($n = 8$) and Nogo-A/B-deficient ($n = 5$) mice. Error bars, mean ± s.e.m. $^{**}P < 0.01$; $^{***}P < 0.001$, unpaired *t*-test (left) or two-way ANOVA followed by Bonferroni's *post hoc* test (right). (**g**) Ach concentration-response curves in the presence or absence of indomethacin (indom) in mesenteric arteries from WT ($n = 11$) and Nogo-A/B-deficient ($n = 6$) mice. Error bars, mean ± s.e.m. $^{***}P < 0.001$, two-way ANOVA. (**h**) Ach concentration-response curves after incubation with indomethacin and L-NAME in mesenteric arteries from WT and Nogo-A/B deficient mice ($n = 5$ per group). (**i**) Left, flow-induced vasodilation without and with L-NAME treatment in mesenteric arteries from WT ($n = 6$) and Nogo-A/B-deficient ($n = 7$) mice. Right, myogenic tone without and with L-NAME treatment in mesenteric arteries from WT ($n = 5$) and Nogo-A/B-deficient ($n = 8$) mice. P, pressure. Error bars, mean ± s.e.m. $^*P < 0.05$; $^{**}P < 0.01$; $^{***}P < 0.001$, two-way ANOVA (right) followed by Bonferroni's *post hoc* test (left). (**j**) Left, L-NAME–induced decrease, compared to baseline, in luminal diameter in carotid arteries from WT and Nogo-A/B-deficient mice ($n = 6$ mice per group); middle, Ach concentration-response curves without or with L-NAME ($n = 6$ per group); right, flow-induced vasodilation without or with L-NAME ($n = 6$ per group). Error bars, mean ± s.e.m. $^*P < 0.05$; $^{**}P < 0.01$; $^{***}P < 0.001$, unpaired *t*-test (left) or two-way ANOVA followed by Bonferroni's *post hoc* test (middle and right).

© 2015 Nature America, Inc. All rights reserved.

These findings were supported by higher plasma levels of nitrites (a breakdown product of NO) and a robust increase in basal and stimulated cyclic guanosine monophosphate (cGMP) levels in Nogo-A/B-deficient aortas as compared to WT (**Fig. 1e**). To confirm these data, we evaluated basal and acetylcholine (Ach)-stimulated eNOS-derived NO in mesenteric arteries mounted in a pressure myograph. We used L-NG-nitroarginine methyl ester (L-NAME) and indomethacin as pharmacological inhibitors of eNOS and cyclooxygenase, respectively, to dissect the role of NO, prostacyclin and endothelium-derived hyperpolarizing factor (EDHF) in Ach-induced vasodilation. Basal and stimulated NO production were markedly increased in mesenteric arteries from Nogo-A/B-deficient mice as compared to controls (**Fig. 1f**). In contrast, the contribution of prostacyclin to vasodilation was significantly smaller in Nogo-A/B-deficient than in WT mesenteric arteries (**Fig. 1g**). EDHF had an equal role in Nogo-A/B-deficient and WT mesenteric arteries, leaving the net response to Ach unchanged (**Fig. 1h**). These results were not surprising, given the compensatory cross-talk between the NO and cyclooxygenase (COX) pathways[26]. These data suggest that endothelial Nogo-B negatively regulates eNOS-derived NO production.

Flow-induced dilation and pressure-induced constriction (myogenic tone) are fundamental mechanisms controlling vascular tone, with flow-induced dilation opposing myogenic tone[27,28]. NO is the major mediator of flow-induced vasorelaxation. In Nogo-A/B-deficient mesenteric arteries, vasodilation in response to a stepwise increase in flow was significantly enhanced compared to WT arteries (**Fig. 1i**). L-NAME treatment blunted flow-induced vasorelaxation in both groups. Conversely, the development of myogenic tone induced by a stepwise increase in pressure was substantially reduced in WT mesenteric arteries in the absence of Nogo-B; L-NAME treatment potentiated the myogenic response to pressure equally in the two groups (**Fig. 1i**). Loss of Nogo-B led to hyperactivation of eNOS and increased flow-induced vasodilation in carotid arteries (**Fig. 1j**). Together, these findings suggest that endothelial Nogo-B has an important role in the regulation of vessel tone via the endothelial NO pathway, such that loss of Nogo-B alters systemic blood pressure.

© 2015 Nature America, Inc. All rights reserved.

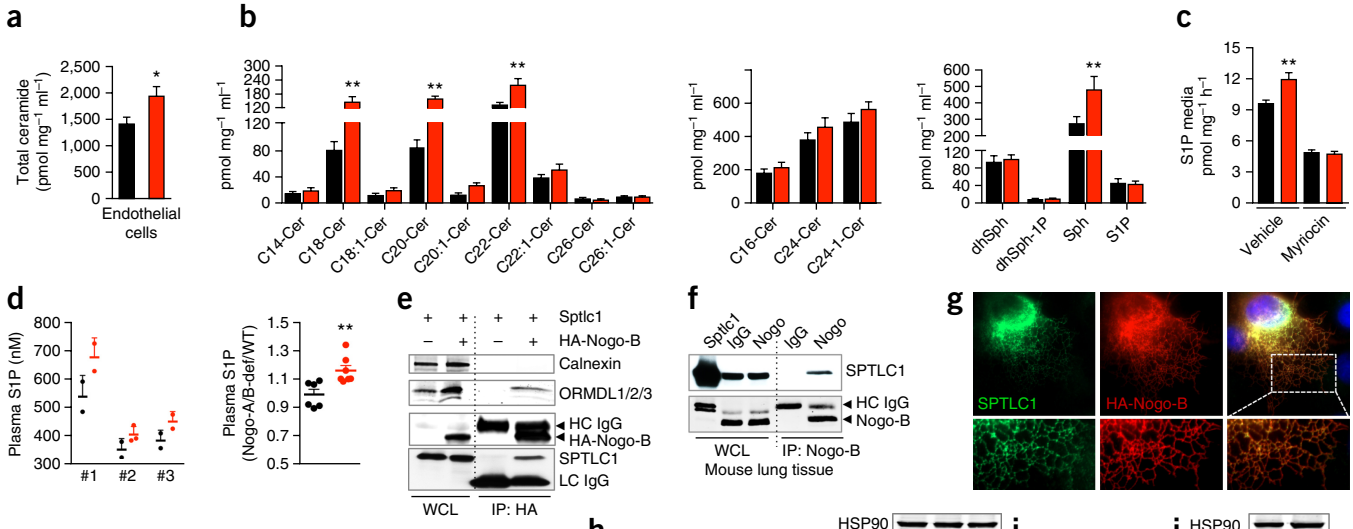

Figure 2 Nogo-B is a negative regulator of sphingolipid *de novo* biosynthesis. (**a**,**b**) Total ceramide levels (**a**) and individual sphingolipid species (**b**) in MLECs from WT and Nogo-A/B-deficient mice, measured by LC-MS. $n = 7$ independent isolations of MLEC per group. dhSph, dihydrosphingosine; Sph, sphingosine. (**c**) S1P concentrations in the culture medium of WT and Nogo-A/B-deficient MLECs treated with vehicle or myriocin ($n = 6$ replicates from 3 independent MLEC isolations per group). (**d**) Left, plasma S1P levels in WT and Nogo-A/B-deficient mice (three independent analyses, #1–#3); right, the same data expressed as fold increase compared to WT levels (WT $n = 6$; Nogo-A/B-deficient, $n = 7$ mice per group). (**e**) Western blot analysis to detect SPTLC1; ORMDL1, ORMDL2 and ORMDL3; calnexin and HA-tagged Nogo-B in whole cell lysates (WCL) or immunoprecipitates with anti-HA agarose (IP: HA) of HEK293T cells transfected with SPTLC1 and HA-tagged Nogo-B or SPTLC1 alone as a control. HC IgG, heavy chain immunoglobulin; LC IgG, light chain immunoglobulin. (**f**) Nogo-B and SPTLC1 coimmunoprecipitation in mouse lung lysates, as assessed by western blot analysis. HEK293T cells overexpressing SPTLC1 were used as a positive control. (**g**) Immunofluorescence staining of COS7 cells transfected with vectors expressing SPTLC1 and HA-tagged Nogo-B. Bottom, magnified view of outlined area (top). (**h**) SPT activity, measured using [^{3}H]serine as substrate followed by TLC separation of sphinganine, in WT and Nogo-A/B-deficient MLECs and HUVECs transfected with Nogo-B siRNA (si-Nogo-B) or control siRNA (si-CTR) and cultured for 72 h (left, $n = 8$ replicates derived from 3 independent experiments per group); and in WT and Nogo-A/B-deficient MLECs treated with lentivirus expressing GFP or HA-tagged Nogo-B (right, $n = 5$, $n = 7$ and $n = 7$ replicates, respectively, derived from 3 independent experiments). Top, western blotting for Nogo-B in HUVECs (left) and in MLECs (right). (**i**,**j**) SPT activity in lung microsomes from WT and Nogo-A/B-deficient mice ($n = 11$ replicates derived from 6 mice per group) (**i**) and in HUVECs transfected with Nogo-B receptor siRNA (si-NgBR) or control siRNA (si-CTR) and cultured for 72 h ($n = 9$ replicates derived from 3 independent experiments) (**j**). The western blot in **j** shows levels of NgBR and HSP90 in HUVECs. Data are expressed as mean ± s.e.m. $^*P < 0.05$; $^{**}P < 0.01$ compared to WT; $^{\#\#}P < 0.01$ compared to control (si-CTR) HUVECs (unpaired *t*-test) (**a**–**d**,**h**–**j**).

Nogo-B negatively regulates sphingolipid synthesis through SPT

Considering the subcellular localization of Nogo-B and eNOS in the tubular ER and the Golgi, respectively, we reasoned that a direct interaction between the two proteins is unlikely. Although it has been suggested that the Rtn4 protein regulates channels responsible for store-operated calcium entry in cultured fibroblasts[29], the equivocal role of these channels in VSMC contractility and the normal contractile responses of Nogo-A/B-deficient mesenteric arteries in response to a variety of vasoconstrictors suggest that Nogo-B is unlikely to regulate calcium signaling in VSMCs. Moreover, Nogo-B does not alter triglyceride synthesis[29]. Given the importance of sphingolipids in controlling blood vessel function[8,9,17,30], we hypothesized that Nogo-B regulates sphingolipid homeostasis.

Quantification of sphingolipid levels by liquid chromatography–tandem mass spectrometry (LC-MS/MS) showed a consistent increase (~30%) in total ceramide levels in the absence of Nogo-B in primary endothelial cells isolated from mouse lung (MLECs) but not in VSMCs (**Fig. 2a**, **Supplementary Fig. 2a**,**b** and **Supplementary Data 2**). This may be due to differential contributions of the *de novo* sphingolipid pathway to sphingolipid levels in endothelial and smooth muscle cells (total ceramide levels were 1,417 ± 108 (s.e.m.) pmol mg^{-1} ml^{-1} in WT MLECs and 850 ± 46 (s.e.m.) pmol mg^{-1} ml^{-1} in WT VSMCs; **Fig. 2a** and **Supplementary Fig. 2a**). Quantification of sphingolipid species in endothelial cells showed that only specific ceramide species, including cer-C18, cer-C20 and cer-C22, were significantly increased in the absence of Nogo-B (**Fig. 2b**), whereas the levels of cer-C16, cer-C24 and

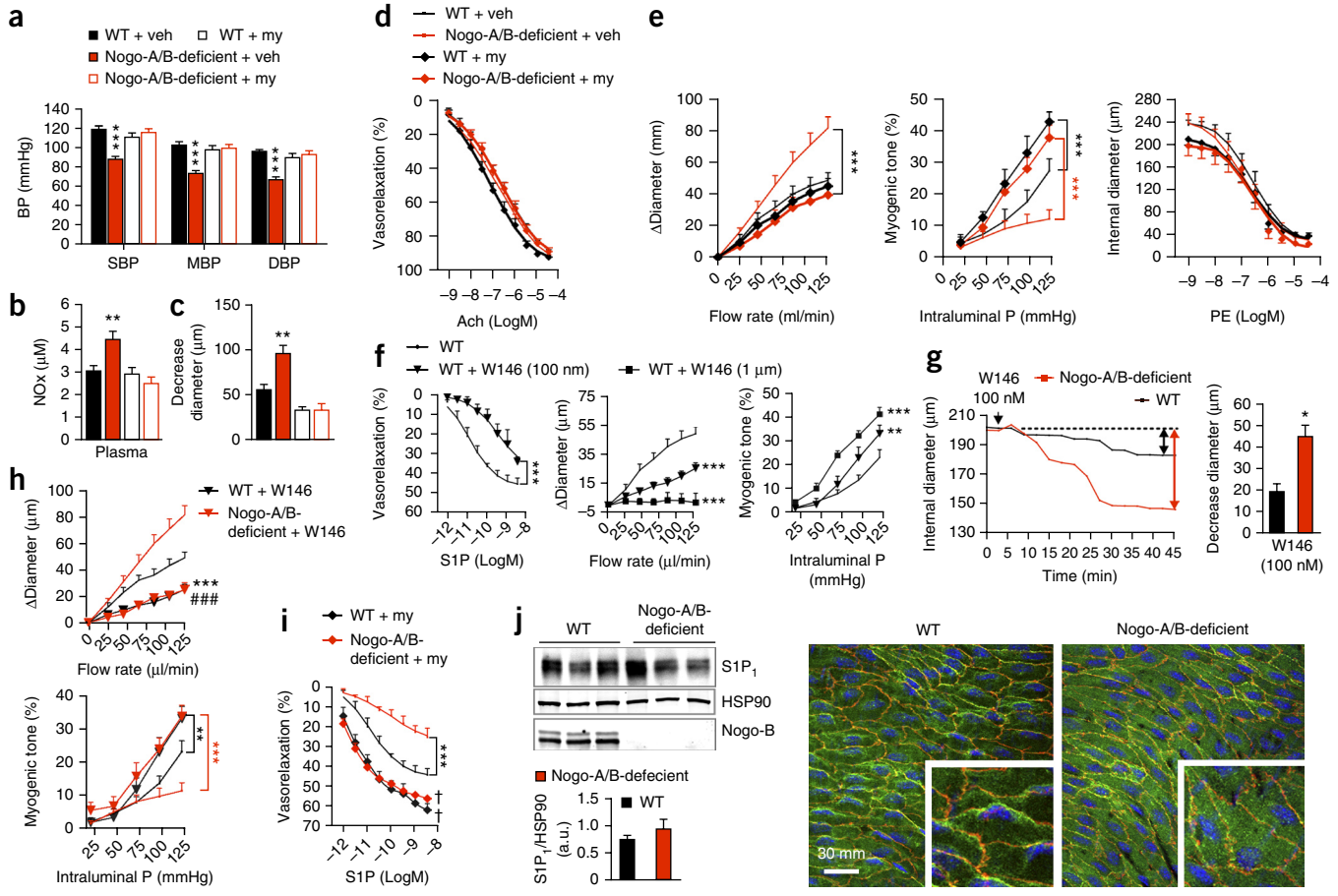

Figure 3 Nogo-B regulates sphingolipid *de novo* biosynthesis to affect blood pressure through S1P-$S1P_1$ signaling. (**a**,**b**) SBP, diastolic blood pressure (DBP) and mean blood pressure (MBP) ($n = 6$ per group) (**a**) and NO plasma levels (NOx) ($n = 5$ WT and $n = 7$ Nogo-A/B-deficient mice) (**b**) in WT and Nogo-A/B-deficient mice 1 d after treatment with myriocin (my, 0.3 mg per kg body weight (mg/kg) intraperitoneally (i.p.) or vehicle (veh, 0.4% fatty acid–free BSA). (**c**–**e**) Mesenteric arteries from the same groups of mice in **a**, assessed for vascular reactivity as follows: (**c**) L-NAME–induced decrease in luminal diameter compared to baseline ($n = 7$ per group), (**d**) Ach-induced vasodilation ($n = 13$ per group) and (**e**) flow-induced vasodilation (left, $n = 5$ per group), myogenic tone (middle, $n = 5$ WT and $n = 7$ Nogo-A/B-deficient arteries) and PE-induced vasoconstriction (right, $n = 6$ WT and $n = 8$ Nogo-A/B-deficient arteries). (**f**) Mesenteric arteries from WT mice incubated with W146 and evaluated for S1P-induced relaxation (left; $n = 4$ per group), flow-induced vasodilation (middle; $n = 5$ per group) and myogenic tone (right; $n = 5$ per group). (**g**,**h**) Mesenteric arteries from WT and Nogo-A/B-deficient mice incubated with W146 or vehicle for 45 min and evaluated for decreased luminal diameter at baseline (**g**; left, representative trace; right, quantification; $n = 9$ WT and $n = 6$ Nogo-A/B-deficient arteries) and flow-induced vasodilation (**h**; left, $n = 5$ WT and $n = 4$ Nogo-A/B-deficient arteries) and myogenic tone (right, $n = 5$ WT and $n = 4$ Nogo-A/B-deficient arteries). (**i**) Vasodilation to S1P in mesenteric arteries from WT ($n = 4$) and Nogo-A/B-deficient ($n = 5$) mice treated with myriocin or vehicle. (**j**) Left, western blot analysis for $S1P_1$ in MLECs from WT and Nogo-A/B-deficient mice. HSP90 was used as a loading control. $n = 4$ independent isolations of MLECs per group. The graph shows densitometric analysis of $S1P_1$ expressed as a ratio to HSP90. Right, immunofluorescence staining of $S1P_1$ in *en face* preparations of WT and Nogo-A/B-deficient aortas. Insets, magnified views. Data are expressed as mean ± s.e.m.; $^{**}P < 0.01$; $^{***}P < 0.001$ compared to WT or as otherwise indicated (**a**–**j**); $^{\#\#\#}P < 0.001$, Nogo-A/B-deficient + W146 vs. Nogo-A/B-deficient (**h**); $^{\dagger}P < 0.001$, myriocin vs. vehicle (**i**). Statistical significance was determined by unpaired *t*-test (**a**,**g**,**j**), one-way ANOVA (**b**,**c**) or two-way ANOVA followed by Bonferroni's *post hoc* test (**e**,**f**,**h**,**i**).

© 2015 Nature America, Inc. All rights reserved.

cer-C24:1 (the most abundant ceramide species, which are involved in apoptosis[31] and survival signaling[32]), were unchanged (**Fig. 2b**). Notably, the levels of sphingosine, a breakdown product of ceramide and a direct precursor of S1P, were markedly higher in Nogo-A/B-deficient MLECs than in WT MLECs (~50%; **Fig. 2b**).

Endothelial cells actively produce and secrete S1P[12], and intracellular S1P levels are tightly controlled by sphingosine kinases and degrading enzymes such as S1P phosphatases and lyase[33]. In the presence of phosphatase inhibitors[12], S1P levels in the culture medium were significantly higher in Nogo-A/B-deficient cells than in WT cells (**Fig. 2c**). Myriocin, a specific inhibitor of SPT, suppressed S1P production in both groups (**Fig. 2c**), suggesting that the *de novo* pathway is responsible for the upregulation of S1P production in the absence of Nogo-B. Significantly higher plasma levels of S1P in Nogo-A/B-deficient mice than in WT mice corroborated these *in vitro* findings (**Fig. 2d**).

Next, we studied the interaction between Nogo-B and SPT, the rate-limiting enzyme of the *de novo* sphingolipid biosynthetic pathway. First, we expressed HA-tagged Nogo-B and SPTLC1, the transmembrane subunit of SPT, in HEK293T cells and found that SPTLC1 coimmunoprecipitated with Nogo-B (**Fig. 2e**). ORMDL[20], a known SPT-interacting protein, coimmunoprecipitated with the Nogo-B–SPT complex, but calnexin did not, indicating that the interaction between SPTLC1 and Nogo-B was specific. Nogo-B was also immunoprecipitated from mouse lung lysate (**Fig. 2f**), indicating an *in vivo* interaction between Nogo-B and SPTLC1. Moreover, the two proteins colocalized in the tubular ER of COS7 cells transfected with SPTLC1 and HA-tagged Nogo-B (**Fig. 2g**). To define the biological function of the Nogo-B–SPT interaction, we measured [^{3}H]serine incorporation into sphinganine (a downstream product of the SPT reaction) in endothelial cells and separated the extracted sphingolipids by thin layer chromatography (TLC) to assess the enzymatic activity of SPT (**Supplementary Fig. 2c–e**). Genetic deficiency of Nogo-B (in MLECs) or small interfering RNA (siRNA)-mediated knockdown of Nogo-B (in human umbilical vein endothelial cells (HUVECs)) led to an increase in SPT activity (**Fig. 2h**), which was restored to WT levels by lentiviral-mediated expression of Nogo-B in Nogo-A/B-deficient MLECs (**Fig. 2h**). To exclude possible effects on [^{3}H]serine uptake, we assayed SPT activity in microsomes isolated from WT and Nogo-A/B-deficient lungs and confirmed that SPT activity was enhanced in the absence of Nogo-A and Nogo-B (**Fig. 2i**). Western blot analysis of WT and Nogo-A/B-deficient microsomes and soluble fractions showed no difference between the two groups in SPTLC1 and calnexin distribution (**Supplementary Fig. 2f**). The Nogo receptor NgBR has been proposed to mediate effects of plasma membrane–localized Nogo-B (<5% of total

© 2015 Nature America, Inc. All rights reserved.

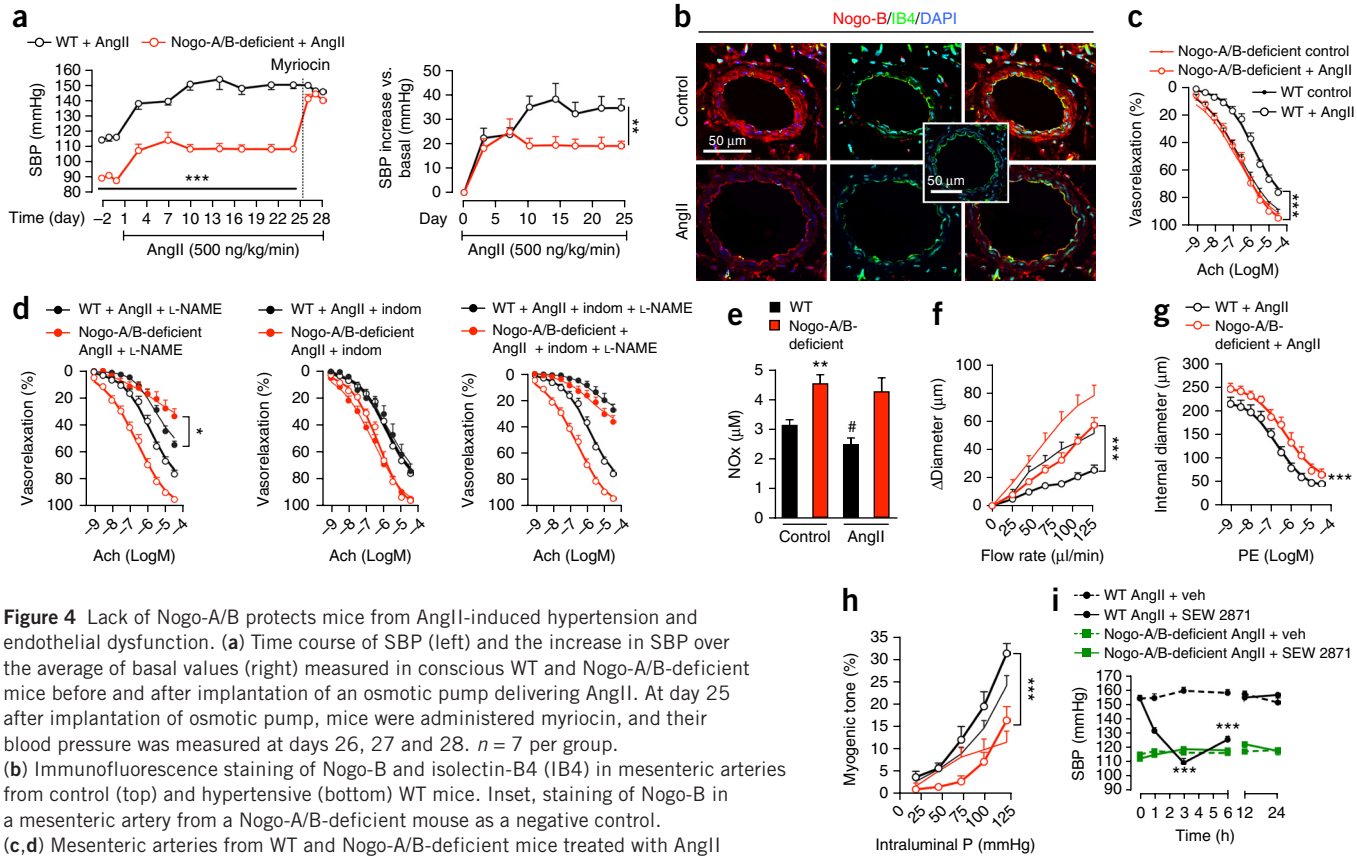

Figure 4 Lack of Nogo-A/B protects mice from AngII-induced hypertension and endothelial dysfunction. (**a**) Time course of SBP (left) and the increase in SBP over the average of basal values (right) measured in conscious WT and Nogo-A/B-deficient mice before and after implantation of an osmotic pump delivering AngII. At day 25 after implantation of osmotic pump, mice were administered myriocin, and their blood pressure was measured at days 26, 27 and 28. $n = 7$ per group. (**b**) Immunofluorescence staining of Nogo-B and isolectin-B4 (IB4) in mesenteric arteries from control (top) and hypertensive (bottom) WT mice. Inset, staining of Nogo-B in a mesenteric artery from a Nogo-A/B-deficient mouse as a negative control. (**c**,**d**) Mesenteric arteries from WT and Nogo-A/B-deficient mice treated with AngII or vehicle (control) and evaluated for (**c**) Ach-induced vasodilation ($n = 16$ WT and $n = 18$ Nogo-A/B-deficient arteries) and (**d**) effects on Ach-induced vasodilation using L-NAME (left, $n = 6$ per group), indomethacin (middle, $n = 8$ per group) and L-NAME plus indomethacin (right, $n = 8$ WT and $n = 6$ Nogo-A/B-deficient arteries). (**e**) Plasma levels of nitrites (NOx) in WT and Nogo-A/B-deficient mice treated with AngII or vehicle ($n = 4$ per group). (**f**–**h**) Mesenteric arteries from WT and Nogo-A/B-deficient mice treated with AngII or vehicle and assessed for (**f**) flow-induced vasodilation ($n = 5$ per group), (**g**) vasoconstriction in response to PE ($n = 9$ WT and $n = 6$ Nogo-A/B-deficient arteries) and (**h**) myogenic tone ($n = 8$ per group). (**i**) WT and Nogo-A/B-deficient mice treated with SEW2871 (3 mg/kg, i.p.) after 4 weeks of chronic infusion of AngII. $n = 7$ per group. Data are expressed as the mean ± s.e.m.; $^*P < 0.05$; $^{**}P < 0.01$; $^{***}P < 0.001$ compared to WT (**a**,**c**–**i**); $^{\#}P < 0.05$ compared to WT control (**e**). Statistical significance was determined by two-way ANOVA followed by Bonferroni's *post hoc* test (**a**,**c**,**d**,**f**–**i**) or one-way ANOVA (**e**).

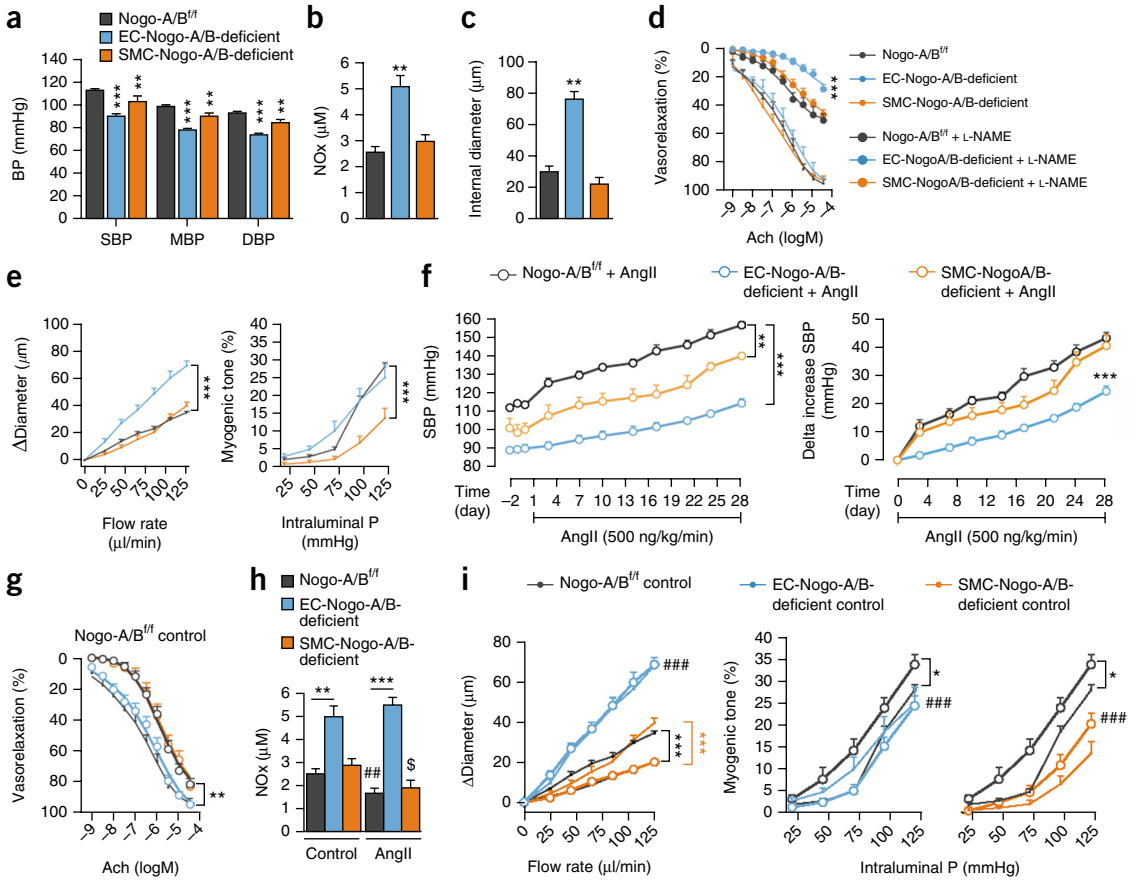

Figure 5 Lack of endothelial Nogo-B protects mice from AngII-induced hypertension and endothelial dysfunction. (**a**,**b**) Nogo-A/B$^{f/f}$, EC-Nogo-A/B-deficient and SMC-Nogo-A/B-deficient mice analyzed for (**a**) SBP, diastolic blood pressure (DBP) and mean blood pressure (MBP) ($n = 15$, $n = 13$ and $n = 14$ respectively per group) and (**b**) plasma NO ($n = 8$ Nogo-A/B$^{f/f}$, $n = 10$ EC-Nogo-A/B-deficient and $n = 10$ SMC-Nogo-A/B-deficient mice). (**c**–**e**) Mesenteric arteries from Nogo-A/B$^{f/f}$, EC-Nogo-A/B-deficient and SMC-Nogo-A/B-deficient mice evaluated for (**c**) L-NAME–induced decrease in luminal diameter versus baseline ($n = 9$ Nogo-A/B$^{f/f}$, $n = 14$ EC-Nogo-A/B-deficient and $n = 7$ SMC-Nogo-A/B-deficient mice), (**d**) vasodilation to Ach without or with L-NAME ($n = 7$ Nogo-A/B$^{f/f}$, $n = 5$ EC-Nogo-A/B-deficient and $n = 6$ SMC-Nogo-A/B-deficient mice) and (**e**) flow-induced vasodilation (left; $n = 7$ Nogo-A/B$^{f/f}$, $n = 8$ EC-Nogo-A/B-deficient and $n = 5$ SMC-Nogo-A/B-deficient mice) and myogenic tone (right; $n = 6$ Nogo-A/B$^{f/f}$, $n = 11$ EC-Nogo-A/B-deficient and $n = 6$ SMC-Nogo-A/B-deficient mice). (**f**) Nogo-A/B$^{f/f}$, EC-Nogo-A/B-deficient and SMC-Nogo-A/B-deficient mice, before and after implantation with osmotic pumps delivering AngII, analyzed for SBP (left) and the increase in SBP over the average of basal values (right; $n = 8$ Nogo-A/B$^{f/f}$, $n = 7$ EC-Nogo-A/B-deficient and $n = 9$ SMC-Nogo-A/B-deficient mice). (**g**) Dose-response curves to Ach of mesenteric arteries from AngII-treated Nogo-A/B$^{f/f}$, EC-Nogo-A/B-deficient and SMC-Nogo-A/B-deficient mice ($n = 8$ Nogo-A/B$^{f/f}$ mice treated with vehicle (control), $n = 10$ Nogo-A/B$^{f/f}$, $n = 9$ EC-Nogo-A/B-deficient and $n = 11$ SMC-Nogo-A/B-deficient mice treated with AngII). (**h**) Plasma levels of nitrites in Nogo-A/B$^{f/f}$, EC-Nogo-A/B-deficient and SMC-Nogo-A/B-deficient mice treated with AngII or vehicle (control) ($n = 8$ Nogo-A/B$^{f/f}$, $n = 7$ EC-Nogo-A/B-deficient and $n = 7$ SMC-Nogo-A/B-deficient mice per condition). (**i**) Mesenteric arteries from Nogo-A/B$^{f/f}$, EC-Nogo-A/B-deficient and SMC-Nogo-A/B-deficient mice treated with AngII or vehicle (control) were assessed for flow-induced vasodilation (left; $n = 7$ Nogo-A/B$^{f/f}$, $n = 8$ EC-Nogo-A/B-deficient and $n = 5$ SMC-Nogo-A/B-deficient mice per control group and $n = 9$ Nogo-A/B$^{f/f}$, $n = 8$ EC-Nogo-A/B-deficient and SMC-Nogo-A/B-deficient mice per AngII group) and myogenic tone (right; $n = 6$ Nogo-A/B$^{f/f}$, $n = 11$ EC-Nogo-A/B-deficient and $n = 6$ SMC-Nogo-A/B-deficient mice per control group, and $n = 6$ Nogo-A/B$^{f/f}$, $n = 11$ EC-Nogo-A/B-deficient and $n = 9$ SMC-Nogo-A/B-deficient mice per AngII group). Data are expressed as mean ± s.e.m.; $^{**}P < 0.01$; $^{***}P < 0.001$ compared to WT (**a**–**i**); $^{\#\#}P < 0.01$, AngII vs. control; $^{\dagger}P < 0.05$, AngII vs. control (**h**); $^{\#\#\#}P < 0.001$, EC-Nogo-A/B-deficient vs. Nogo-A/B$^{f/f}$ (**i**). Statistical significance was determined by one-way ANOVA (**a**–**c**,**h**) or two-way ANOVA followed by Bonferroni's *post hoc* test (**d**–**g**,**i**).

Nogo-B) on vascular function[25]. Notably, siRNA-mediated knockdown of NgBR did not alter the activity of SPT in HUVECs (**Fig. 2j**), suggesting that the intracellular regulation of *de novo* sphingolipid biosynthesis by Nogo-B is not mediated by NgBR.

Nogo-B binds SPT to regulate blood pressure through S1P-S1P$_1$ axis

To confirm the causal role of sphingolipid upregulation in the hypotension observed in Nogo-A/B-deficient mice, we inhibited SPT activity *in vivo* with myriocin[34] and measured physiological outcomes. In Nogo-A/B-deficient mice, a single dose of myriocin normalized blood pressure (**Fig. 3a**), NO plasma levels (**Fig. 3b**) and basal tone in mesenteric arteries *ex vivo* (**Fig. 3c**), whereas myriocin treatment did not affect the contributions of NO, prostacyclin and EDHF to Ach-induced vasodilation (**Fig. 3d**, **Supplementary Fig. 3a** and **Supplementary Data 3**). Further, myriocin abolished the difference in flow-induced dilation between WT and Nogo-A/B-deficient mesenteric arteries and increased myogenic tone to the same degree in both groups (**Fig. 3e**). Myriocin did not alter the response of arteries to PE, but increased basal tone in both groups, probably owing to diminished basal eNOS activation (**Fig. 3e**). These results indicate that upregulation of the *de novo* sphingolipid biosynthetic pathway is the major mechanism responsible for the decrease in vascular

© 2015 Nature America, Inc. All rights reserved.

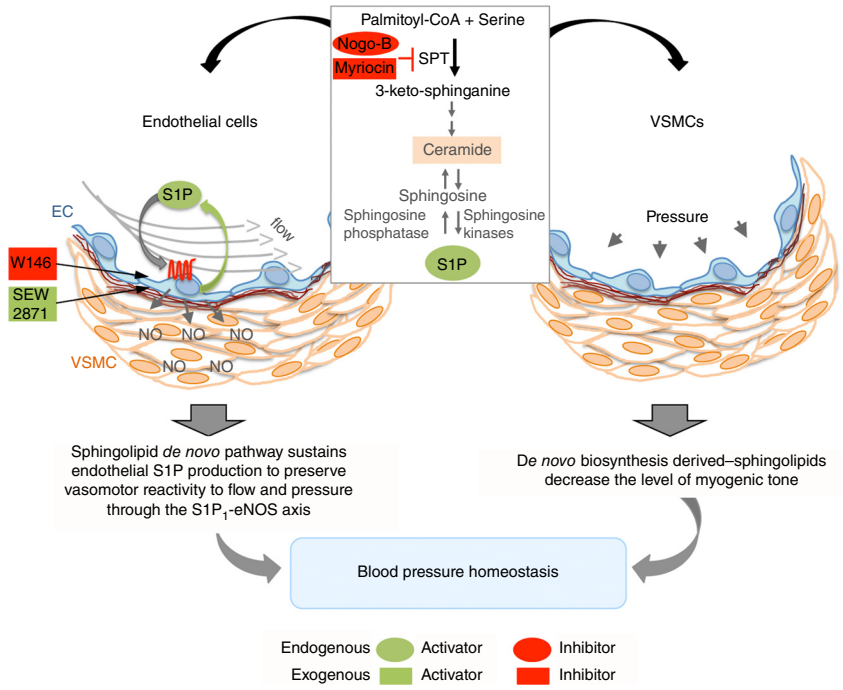

Figure 6 Endothelial Nogo-B is a critical mediator of hypertension and vascular dysfunction through negative regulation of sphingolipid *de novo* biosynthesis. Endothelial-derived S1P has a crucial function in flow-mediated vasodilation through an autocrine $S1P_1$-eNOS signaling axis. S1P is transported out of endothelial cells, where it activates $S1P_1$-eNOS pathway in an autocrine fashion, leading to NO production and blood pressure regulation. Left, in the absence of Nogo-B, SPT activity is enhanced and endothelial cells produce increased amounts of S1P, resulting in increased flow-mediated vasodilation and decreased basal tone. Myriocin, a specific inhibitor of SPT, and W146, an $S1P_1$ antagonist, reinstate the normal response to blood flow and pressure in Nogo-A/B-deficient resistance arteries. SEW2871, an agonist of $S1P_1$, lowers blood pressure in hypertensive mice. Right, the lack of Nogo-B in smooth muscle cells leads to an increase in sphingolipid biosynthesis and ceramide levels, resulting in decreased myogenic tone. EC, endothelial cell.

resistance and hypotension in Nogo-A/B-deficient mice, through regulation of flow-mediated vasodilation and myogenic tone.

S1P produced in the endothelium is transported out of the cell to activate the $S1P_1$-eNOS pathway[12,30]. eNOS-derived NO is a major effector of S1P-mediated $S1P_1$ activation (**Supplementary Fig. 3b**). To investigate more directly the role of autocrine S1P-$S1P_1$-eNOS signaling in endothelial cells in the regulation of vascular tone, we used W146, a known antagonist of $S1P_1$ (half-maximal inhibitory concentration (IC_{50}) of 70 nM) (**Fig. 3f**). In WT mesenteric arteries, W146 treatment reduced basal eNOS activation and increased basal tone and vasoconstriction in response to PE (**Supplementary Fig. 3c–e**), whereas it did not affect the contributions of prostacyclin, NO and EDHF to Ach-induced vasodilation (**Supplementary Fig. 3f,g**). Notably, at a concentration of 1 μM, W146 blunted flow-mediated vasodilation and significantly increased myogenic tone in WT mesenteric arteries (**Fig. 3f**). The importance of $S1P_1$ to the flow-mediated response has previously been reported for endothelial cells in culture[12]. Our results with W146 demonstrate the direct role of $S1P_1$ receptors in the response to blood flow in resistance vessels and implicate an augmented myogenic tone as a counteracting response to the loss of flow-induced vasodilation.

On the basis of these findings, we hypothesized that an endothelial S1P-$S1P_1$-eNOS autocrine loop is upregulated in Nogo-A/B-deficient mesenteric arteries and that this upregulation accounts for the increase in flow-induced dilation and NO release. In this scenario, we would expect high activation of $S1P_1$ receptors in Nogo-A/B-deficient mesenteric arteries under baseline conditions. Indeed, the increase of vascular tone was greater in Nogo-A/B-deficient than in WT mesenteric arteries after W146 treatment (**Fig. 3g**), indicating a gain of $S1P_1$ signaling in the absence of Nogo-B. Notably, partial inhibition of $S1P_1$ by W146 normalized the flow response and myogenic tone of Nogo-A/B-deficient mesenteric arteries (**Fig. 3h**). Upregulation of an S1P-$S1P_1$-eNOS autocrine loop in absence of Nogo-A and Nogo-B was further corroborated by the observation that S1P-induced vasodilation was markedly reduced in Nogo-A/B-deficient mesenteric arteries as compared to WT (**Fig. 3i**). Moreover, myriocin treatment increased the sensitivity of WT and Nogo-A/B-deficient mesenteric arteries to S1P to the same degree (**Fig. 3i**), and $S1P_1$ expression was similar between the two groups (**Fig. 3j**). Taken together, these findings suggest a protective role of S1P signaling and indicate that hyperactivation of endothelial S1P-$S1P_1$-eNOS autocrine signaling accounts for the reduced vascular tone observed in the absence of Nogo-B.

Nogo-B mediates vascular dysfunction in hypertension

To assess the importance of Nogo-B in pathological conditions, we employed the angiotensin II (AngII)-induced model of hypertension, which recapitulates features of human hypertension, including vascular dysfunction[35–37]. Chronic infusion of AngII produced robust and sustained hypertension in WT mice, whereas it induced only a mild increase in blood pressure in Nogo-A/B-deficient mice (**Fig. 4a**). Notably, myriocin administration raised the blood pressure of AngII-treated Nogo-A/B-deficient mice to that of AngII-treated WT mice (**Fig. 4a**).

Immunofluorescence staining of mesenteric arteries revealed that Nogo-B was expressed in both endothelial cells and VSMCs in vehicle-treated WT mice and that Nogo-B levels were much lower in VSMCs but unchanged in endothelial cells in the mesenteric arteries of hypertensive (AngII-treated WT) mice (**Fig. 4b**). These findings suggest that Nogo-B exerts pro-hypertensive effects in endothelial cells rather than in VSMCs.

Consistent with these *in vivo* findings, mesenteric arteries from AngII-treated Nogo-A/B-deficient mice were protected from endothelial dysfunction, showing preserved vasorelaxation in response to Ach and preserved NO production, with no difference in the contribution of prostacyclin and EDHF to Ach-induced vasodilation (**Fig. 4c–e**), and a sustained vasodilatory response to blood flow (**Fig. 4f**). Mesenteric arteries from WT mice showed greater myogenic tone and increased vasoconstriction in response to PE than did those from Nogo-A/B-deficient mice (**Fig. 4g,h**).

Finally, to directly assess the protective role of $S1P_1$ signaling in hypertension, we injected AngII-treated WT and Nogo-A/B-deficient mice with SEW2871, a selective agonist of $S1P_1$. SEW2871 administration

© 2015 Nature America, Inc. All rights reserved.

led to a marked hypotensive response in WT but not Nogo-A/B-deficient mice; the blood pressure of AngII-treated Nogo-A/B-deficient mice was close to normal values (**Fig. 4i**). These data demonstrate that in a hypertensive model, Nogo-B negatively regulates the *de novo* pathway of sphingolipid biosynthesis in the vasculature, leading to endothelial dysfunction and higher blood pressure.

Endothelial Nogo-B promotes vascular dysfunction and hypertension

To dissect the roles of Nogo-B in endothelial and smooth muscle cells, we generated mice lacking Nogo-A and Nogo-B specifically in endothelial cells or in smooth muscle cells. We first generated mice with a *lox*P-flanked allele of the gene encoding Nogo-A and Nogo-B (Nogo-A/B$^{f/f}$). We then bred these mice to mice expressing Cre recombinase specifically in endothelial or smooth muscle cells to generate endothelial cell (EC)- or smooth muscle cell (SMC)-Nogo-A/B-deficient mice (Online Methods). We documented a near-complete loss of Nogo-B mRNA expression and protein expression in endothelial cells and smooth muscle cells in EC-Nogo-A/B-deficient and SMC-Nogo-A/B-deficient mice, respectively (**Supplementary Fig. 4a–g** and **Supplementary Data 4**). As reported by other groups[25,38], Nogo-A is not detectable in endothelial cells; thus, the phenotype observed in EC-Nogo-A/B-deficient mice can be ascribed to the specific loss of Nogo-B.

The lack of Nogo-B in endothelial cells and, to a lesser extent, in smooth muscle cells, led to a marked reduction in baseline blood pressure (**Fig. 5a**), recapitulating the effects observed in systemic Nogo-A/B-deficient mice and suggesting that Nogo-B acts predominantly in endothelial cells to regulate systemic blood pressure. We observed increased plasma levels of NO and increased basal and Ach-stimulated production of NO in mesenteric arteries specifically in EC-Nogo-A/B-deficient mice, whereas myogenic tone (but not PE-induced vasoconstriction) (**Supplementary Fig. 4h**) was significantly reduced in mesenteric arteries from SMC-Nogo-A/B-deficient mice (**Fig. 5b–e**). These results indicate that endothelial Nogo-B affects flow-induced vasodilation through the S1P-S1P$_1$-eNOS axis, whereas smooth muscle Nogo-B regulates myogenic tone. EC-Nogo-A/B-deficient mice were protected from AngII-induced hypertension and endothelial dysfunction, with preserved production of NO under baseline and Ach-stimulated conditions, and had a preserved vasodilatory response to flow (**Fig. 5f–i**). AngII-treated SMC-Nogo-A/B-deficient mice developed a milder hypertension than did Nogo-A/B$^{f/f}$ control mice, probably because of a reduced myogenic tone; however, SMC-Nogo-A/B-deficient mice showed endothelial dysfunction and impaired flow-mediated vasodilation, similarly to control Nogo-A/B$^{f/f}$ mice (**Fig. 5f–i**). Ceramide-activated serine-threonine phosphatases (CAPPs) such as phosphatase 1 (PP1) and phosphatase 2A (PP2A), which have a defined role in smooth muscle cell contractility[39], have been found to interact with ceramide[40]. Increased levels of cer-C18, cer-C20 and cer-C22 in smooth muscle cells of SMC-Nogo-A/B-deficient mice may therefore be responsible for the reduced myogenic tone observed in these mice. Together, these findings suggest that Nogo-B, acting predominantly in endothelial cells, contributes to vascular dysfunction and hypertension (**Fig. 6**).

DISCUSSION

Dysfunction of the endothelium is associated with hypertensive cardiovascular disease and probably precedes its development[3,41]. Recently, bioactive sphingolipids, and S1P in particular, have been shown to regulate important aspects of cardiovascular pathophysiology, including angiogenesis, vascular tone and endothelial barrier integrity[42–44]. Although altered sphingolipid signaling has been implicated in endothelial dysfunction and cardiovascular disease[42,45], the specific molecular mechanisms involved are still poorly understood.

Our study identifies Nogo-B as a negative regulator of the *de novo* pathway of sphingolipid biosynthesis, independently of NgBR[46]. We found that Nogo-B binds to and inhibits the activity of SPT, the rate-limiting enzyme of the pathway. Thus, loss of a Nogo-B–mediated brake on SPT leads to an increase in locally produced sphingolipids and S1P in the endothelium, exerting vasculoprotective effects.

Indeed, S1P is a potent activator of eNOS through S1P$_1$ and S1P$_3$, and many of the beneficial effects of S1P on the vasculature are mediated by NO, including cell survival, proliferation and migration[47,48]. Our data on the S1P$_1$ antagonist W146 corroborate the role of S1P$_1$ in blood flow–induced dilation in resistance vessels and provide direct evidence of the importance of endothelial-derived S1P in controlling vascular response to flow through an autocrine-paracrine loop involving S1P$_1$-eNOS signaling.

To date, the impact of S1P receptor modulators on cardiovascular pathophysiology remains largely unexplored. Here, we reveal antihypertensive effects of S1P$_1$ signaling, identifying a potential therapeutic target for the treatment of this pathological condition. Recently S1P receptor modulation has become an attractive pharmacological target[49–51]. Our findings suggest that potential cardiovascular effects should be a consideration in the development of such agents.

Although much attention has been devoted to the sphingolipid recycling pathway and the role of sphingomyelinase in cardiovascular disease[52], relatively little attention has been paid to the function of the *de novo* pathway in this context. Our studies reveal a protective function of the *de novo* pathway within the vasculature in the pathogenesis of hypertension. The production of endothelial S1P is strongly sustained by the *de novo* pathway; indeed, we found that the SPT inhibitor myriocin reduced S1P levels in the culture medium of endothelial cells by ~50% after only 4 h of incubation, and a single dose of myriocin normalized the blood pressure of Nogo-A/B-deficient mice and restored blood flow–induced vasodilation, myogenic tone and NO production of mesenteric arteries. Our pharmacological data using the S1P$_1$ antagonist W146 and an SPT inhibitor myriocin indicate the importance of local S1P-S1P$_1$-eNOS signaling in the regulation of vascular tone in both normal physiology and hypertension. Moreover, the ability of the selective S1P$_1$ antagonist SEW2871 to normalize blood pressure in hypertensive mice reveals the critical role of S1P$_1$-mediated signaling in hypertension.

Genome-wide association studies have identified a strong association between the *ORMDL* locus and the incidence of childhood asthma[22], and Orm proteins in yeast (ORMDL proteins in human) have recently been identified as negative regulators of SPT[20]. We found that ORMDL coimmunoprecipitated with Nogo-B and SPTLC1, suggesting that these proteins are part of the same complex. Moreover, Nogo-A and Nogo-B deficiency led to an increase in microsomal SPT activity in the lung, suggesting that Nogo-B is a regulatory factor of SPT.

Despite expression of Nogo-B in both endothelial and smooth muscle cells, Nogo-B has a selective impact on sphingolipid synthesis in endothelial cells, particularly with respect to the steady-state levels of cer-C18, cer-C20 and cer-C22. This selective effect may be due to differential contributions of the *de novo* pathway of sphingolipid biosynthesis in endothelial cells and VSMCs, differential regulation of sphingolipid biosynthesis depending on cell type and pathological conditions, or cell type–specific functioning of Nogo-B.

Our findings in resistance arteries from systemic and EC-Nogo-A/B-deficient mice indicate the important role of Nogo-B in vascular tone regulation by control of local sphingolipid production. In a recent study,

© 2015 Nature America, Inc. All rights reserved.

a specific extracellular domain of Nogo-A was proposed to activate $S1P_2$ in the brain[53]. The $S1P_2$ receptor is also expressed in VSMCs[11]; however, Nogo-A is undetectable in the mouse aorta and femoral artery[25], excluding the possibility that the vascular phenotype of Nogo-A/B-deficient mesenteric and carotid arteries is due to lack of Nogo-A–mediated signaling in the vasculature. Although our data in Nogo-A/B-deficient mice do not rule out a possible contribution of Nogo-A, which is enriched in the brain, in the control of blood pressure, the hypotension of EC-Nogo-A/B-deficient mice and their resistance to hypertension and vascular dysfunction can be attributed to endothelial-expressed Nogo-B.

The finding that Nogo-B regulates sphingolipid signaling provides a framework for investigating whether alterations of Nogo activity and sphingolipid metabolism contribute to other pathological conditions that have been reported in mice lacking Nogo-B, including vascular injury[25], asthma[54] and liver fibrosis[55] and inflammation[56]. The observation that Nogo-B controls sphingolipid metabolism strongly suggests that dysregulation of this signaling pathway may have a causative role in the pathogenesis of hypertension and endothelial dysfunction leading to cardiovascular disease. Most notably, the identification of regulatory mechanisms for endothelial sphingolipid production may allow for targeted pharmacological intervention of these pathways in cardiovascular disease.

METHODS

Methods and any associated references are available in the online version of the paper.

Note: Any Supplementary Information and Source Data files are available in the online version of the paper.

ACKNOWLEDGMENTS

This work was supported by European Cooperation in Science and Technology (COST) Action BM1005 European Network on Gasotransmitters (ENOG) to M.B.; US National Institutes of Health (NIH) R37-HL67330 and R01HL89934 to T.H.; NIH R01HL126913-01, a Harold S. Geneen Charitable Trust Award for Coronary Heart Disease Research and American Heart Association grant 11SDG5710010 to A.D.L.

AUTHOR CONTRIBUTIONS

A.C. and Y.Z. designed and carried out experiments, analyzed results and contributed to writing the manuscript. M.K. contributed with preparation of WT and Nogo-A/B-deficient MLEC for sphingolipid measurements. H.O. prepared HA-tagged-Nogo-B lentivirus. S.G. performed all the *en face* mouse aorta preparations, staining and imaging. M.B. helped in designing experiments and interpretation of results. F.J.G. contributed to designing experiments and discussion of results. X.-C. J. contributed to and oversaw the SPT enzymatic assays. T.H. contributed to design of experiments and interpretation of results and provided feedback on the manuscript. A.D.L. designed experiments, interpreted results and wrote the manuscript.

COMPETING FINANCIAL INTERESTS

The authors declare no competing financial interests.

Reprints and permissions information is available online at http://www.nature.com/reprints/index.html.

1. Kearney, P.M. *et al.* Global burden of hypertension: analysis of worldwide data. *Lancet* **365**, 217–223 (2005).
2. Vanhoutte, P.M. Endothelial dysfunction in hypertension. *J. Hypertens. Suppl.* **14**, S83–S93 (1996).
3. Taddei, S. & Salvetti, A. Pathogenetic factors in hypertension. Endothelial factors. *Clin. Exp. Hypertens.* **18**, 323–335 (1996).
4. Taddei, S. *et al.* Defective L-arginine-nitric oxide pathway in offspring of essential hypertensive patients. *Circulation* **94**, 1298–1303 (1996).
5. Huang, P.L. *et al.* Hypertension in mice lacking the gene for endothelial nitric oxide synthase. *Nature* **377**, 239–242 (1995).
6. Haynes, W.G., Noon, J.P., Walker, B.R. & Webb, D.J. L-NMMA increases blood pressure in man. *Lancet* **342**, 931–932 (1993).
7. Aisaka, K., Gross, S.S., Griffith, O.W. & Levi, R. NG-methylarginine, an inhibitor of endothelium-derived nitric oxide synthesis, is a potent pressor agent in the guinea pig: does nitric oxide regulate blood pressure *in vivo*? *Biochem. Biophys. Res. Commun.* **160**, 881–886 (1989).
8. Dantas, A.P., Igarashi, J. & Michel, T. Sphingosine 1-phosphate and control of vascular tone. *Am. J. Physiol. Heart Circ. Physiol.* **284**, H2045–H2052 (2003).
9. Igarashi, J. & Michel, T. S1P and eNOS regulation. *Biochim. Biophys. Acta* **1781**, 489–495 (2008).
10. Salomone, S. *et al.* S1P3 receptors mediate the potent constriction of cerebral arteries by sphingosine-1-phosphate. *Eur. J. Pharmacol.* **469**, 125–134 (2003).
11. Coussin, F., Scott, R.H., Wise, A. & Nixon, G.F. Comparison of sphingosine 1-phosphate-induced intracellular signaling pathways in vascular smooth muscles: differential role in vasoconstriction. *Circ. Res.* **91**, 151–157 (2002).
12. Venkataraman, K. *et al.* Vascular endothelium as a contributor of plasma sphingosine 1-phosphate. *Circ. Res.* **102**, 669–676 (2008).
13. Hänel, P., Andreani, P. & Graler, M.H. Erythrocytes store and release sphingosine 1-phosphate in blood. *FASEB J.* **21**, 1202–1209 (2007).
14. Camerer, E. *et al.* Sphingosine-1-phosphate in the plasma compartment regulates basal and inflammation-induced vascular leak in mice. *J. Clin. Invest.* **119**, 1871–1879 (2009).
15. Young, R.M. *et al.* Zebrafish yolk-specific not really started (*nrs*) gene is a vertebrate homolog of the *Drosophila* spinster gene and is essential for embryogenesis. *Dev. Dyn.* **223**, 298–305 (2002).
16. Tauseef, M. *et al.* Activation of sphingosine kinase-1 reverses the increase in lung vascular permeability through sphingosine-1-phosphate receptor signaling in endothelial cells. *Circ. Res.* **103**, 1164–1172 (2008).
17. Jung, B. *et al.* Flow-regulated endothelial S1P receptor-1 signaling sustains vascular development. *Dev. Cell* **23**, 600–610 (2012).
18. Nagiec, M.M., Baltisberger, J.A., Wells, G.B., Lester, R.L. & Dickson, R.C. The *LCB2* gene of *Saccharomyces* and the related *LCB1* gene encode subunits of serine palmitoyltransferase, the initial enzyme in sphingolipid synthesis. *Proc. Natl. Acad. Sci. USA* **91**, 7899–7902 (1994).
19. Hanada, K. *et al.* Sphingolipids are essential for the growth of Chinese hamster ovary cells. Restoration of the growth of a mutant defective in sphingoid base biosynthesis by exogenous sphingolipids. *J. Biol. Chem.* **267**, 23527–23533 (1992).
20. Breslow, D.K. *et al.* Orm family proteins mediate sphingolipid homeostasis. *Nature* **463**, 1048–1053 (2010).
21. Han, S., Lone, M.A., Schneiter, R. & Chang, A. Orm1 and Orm2 are conserved endoplasmic reticulum membrane proteins regulating lipid homeostasis and protein quality control. *Proc. Natl. Acad. Sci. USA* **107**, 5851–5856 (2010).
22. Moffatt, M.F. *et al.* Genetic variants regulating ORMDL3 expression contribute to the risk of childhood asthma. *Nature* **448**, 470–473 (2007).
23. Kim, J.E., Li, S., GrandPre, T., Qiu, D. & Strittmatter, S.M. Axon regeneration in young adult mice lacking Nogo-A/B. *Neuron* **38**, 187–199 (2003).
24. Zheng, B. *et al.* Lack of enhanced spinal regeneration in Nogo-deficient mice. *Neuron* **38**, 213–224 (2003).
25. Acevedo, L. *et al.* A new role for Nogo as a regulator of vascular remodeling. *Nat. Med.* **10**, 382–388 (2004).
26. Beverelli, F., Bea, M.L., Puybasset, L., Giudicelli, J.F. & Berdeaux, A. Chronic inhibition of NO synthase enhances the production of prostacyclin in coronary arteries through upregulation of the cyclooxygenase type 1 isoform. *Fundam. Clin. Pharmacol.* **11**, 252–259 (1997).
27. Davies, P.F. Flow-mediated endothelial mechanotransduction. *Physiol. Rev.* **75**, 519–560 (1995).
28. Bevan, J.A. & Henrion, D. Pharmacological implications of the flow-dependence of vascular smooth muscle tone. *Annu. Rev. Pharmacol. Toxicol.* **34**, 173–190 (1994).
29. Jozsef, L. *et al.* Reticulon 4 is necessary for endoplasmic reticulum tubulation, STIM1-ORAI1 coupling, and store-operated calcium entry. *J. Biol. Chem.* **289**, 9380–9395 (2014).
30. Igarashi, J. & Michel, T. Agonist-modulated targeting of the EDG-1 receptor to plasmalemmal caveolae. eNOS activation by sphingosine 1-phosphate and the role of caveolin-1 in sphingolipid signal transduction. *J. Biol. Chem.* **275**, 32363–32370 (2000).
31. Mesicek, J. *et al.* Ceramide synthases 2, 5, and 6 confer distinct roles in radiation-induced apoptosis in HeLa cells. *Cell. Signal.* **22**, 1300–1307 (2010).
32. Pewzner-Jung, Y. *et al.* A critical role for ceramide synthase 2 in liver homeostasis: II. insights into molecular changes leading to hepatopathy. *J. Biol. Chem.* **285**, 10911–10923 (2010).
33. Bolz, S.S. *et al.* Sphingosine kinase modulates microvascular tone and myogenic responses through activation of RhoA/Rho kinase. *Circulation* **108**, 342–347 (2003).
34. Hanada, K., Nishijima, M., Fujita, T. & Kobayashi, S. Specificity of inhibitors of serine palmitoyltransferase (SPT), a key enzyme in sphingolipid biosynthesis, in intact cells. A novel evaluation system using an SPT-defective mammalian cell mutant. *Biochem. Pharmacol.* **59**, 1211–1216 (2000).
35. Rajagopalan, S. *et al.* Angiotensin II-mediated hypertension in the rat increases vascular superoxide production via membrane NADH/NADPH oxidase activation. Contribution to alterations of vasomotor tone. *J. Clin. Invest.* **97**, 1916–1923 (1996).

© 2015 Nature America, Inc. All rights reserved.

36. Lais, L.T. & Brody, M.J. Vasoconstrictor hyperresponsiveness: an early pathogenic mechanism in the spontaneously hypertensive rat. *Eur. J. Pharmacol.* **47**, 177–189 (1978).
37. Tang, K.M. *et al.* Regulator of G-protein signaling-2 mediates vascular smooth muscle relaxation and blood pressure. *Nat. Med.* **9**, 1506–1512 (2003).
38. Wälchli, T. *et al.* Nogo-A is a negative regulator of CNS angiogenesis. *Proc. Natl. Acad. Sci. USA* **110**, E1943–E1952 (2013).
39. Butler, T., Paul, J., Europe-Finner, N., Smith, R. & Chan, E.C. Role of serine-threonine phosphoprotein phosphatases in smooth muscle contractility. *Am. J. Physiol. Cell Physiol.* **304**, C485–C504 (2013).
40. Hannun, Y.A. Functions of ceramide in coordinating cellular responses to stress. *Science* **274**, 1855–1859 (1996).
41. Celermajer, D.S. *et al.* Non-invasive detection of endothelial dysfunction in children and adults at risk of atherosclerosis. *Lancet* **340**, 1111–1115 (1992).
42. Theilmeier, G. *et al.* High-density lipoproteins and their constituent, sphingosine-1-phosphate, directly protect the heart against ischemia/reperfusion injury *in vivo* via the S1P3 lysophospholipid receptor. *Circulation* **114**, 1403–1409 (2006).
43. Obinata, H. & Hla, T. Sphingosine 1-phosphate in coagulation and inflammation. *Semin. Immunopathol.* **34**, 73–91 (2012).
44. Nofer, J.R. *et al.* FTY720, a synthetic sphingosine 1 phosphate analogue, inhibits development of atherosclerosis in low-density lipoprotein receptor-deficient mice. *Circulation* **115**, 501–508 (2007).
45. Jiang, X.C., Goldberg, I.J. & Park, T.S. Sphingolipids and cardiovascular diseases: lipoprotein metabolism, atherosclerosis and cardiomyopathy. *Adv. Exp. Med. Biol.* **721**, 19–39 (2011).
46. Miao, R.Q. *et al.* Identification of a receptor necessary for Nogo-B stimulated chemotaxis and morphogenesis of endothelial cells. *Proc. Natl. Acad. Sci. USA* **103**, 10997–11002 (2006).
47. Rikitake, Y. *et al.* Involvement of endothelial nitric oxide in sphingosine-1-phosphate-induced angiogenesis. *Arterioscler. Thromb. Vasc. Biol.* **22**, 108–114 (2002).
48. Igarashi, J., Miyoshi, M., Hashimoto, T., Kubota, Y. & Kosaka, H. Hydrogen peroxide induces S1P1 receptors and sensitizes vascular endothelial cells to sphingosine 1-phosphate, a platelet-derived lipid mediator. *Am. J. Physiol. Cell Physiol.* **292**, C740–C748 (2007).
49. Chun, J. & Hartung, H.P. Mechanism of action of oral fingolimod (FTY720) in multiple sclerosis. *Clin. Neuropharmacol.* **33**, 91–101 (2010).
50. Cohen, J.A. *et al.* Oral fingolimod or intramuscular interferon for relapsing multiple sclerosis. *N. Engl. J. Med.* **362**, 402–415 (2010).
51. Kappos, L. *et al.* A placebo-controlled trial of oral fingolimod in relapsing multiple sclerosis. *N. Engl. J. Med.* **362**, 387–401 (2010).
52. Pavoine, C. & Pecker, F. Sphingomyelinases: their regulation and roles in cardiovascular pathophysiology. *Cardiovasc. Res.* **82**, 175–183 (2009).
53. Kempf, A. *et al.* The sphingolipid receptor S1PR2 is a receptor for Nogo-a repressing synaptic plasticity. *PLoS Biol.* **12**, e1001763 (2014).
54. Wright, P.L. *et al.* Epithelial reticulon 4B (Nogo-B) is an endogenous regulator of Th2-driven lung inflammation. *J. Exp. Med.* **207**, 2595–2607 (2010).
55. Zhang, D. *et al.* Reticulon 4B (Nogo-B) is a novel regulator of hepatic fibrosis. *Hepatology* **53**, 1306–1315 (2011).
56. Di Lorenzo, A., Manes, T.D., Davalos, A., Wright, P.L. & Sessa, W.C. Endothelial reticulon-4B (Nogo-B) regulates ICAM-1-mediated leukocyte transmigration and acute inflammation. *Blood* **117**, 2284–2295 (2011).

© 2015 Nature America, Inc. All rights reserved.

ONLINE METHODS

Animals. Nogo-A/B-deficient mice were generated as previously described[24]. To generate Nogo-A/B$^{f/f}$ mice, we inserted *loxP* sites into the *Rtn4* gene to flank exons 2 and 3; the targeted region was about 3.29 kb in length. The proximal *loxP* cassette was placed 186 bp upstream of exon 2, in intron 1–2, and the distal *loxP* cassette was placed 237 bp downstream of exon 3, in intron 3–4.

Mice lacking Nogo-A/B specifically in endothelial cells (EC-Nogo-A/B-deficient) were obtained by crossing Nogo-A/B$^{f/f}$ mice with transgenic mice in which the VE-cadherin promoter drives expression of tamoxifen-responsive Cre (VE-Cad-CreERT2)[57] such that tamoxifen treatment selectively deletes the *lox*P-flanked ('floxed') region of *Rtn4* in endothelial cells. Mice lacking Nogo-A/B specifically in smooth muscle cells (SMC-NogoA/B-deficient) were obtained by crossing Nogo-A/B$^{f/f}$ mice with transgenic mice in which the α-smooth muscle actin promoter drives expression of Cre (SM22α-Cre) (Tagln-Cre 1Her/J, The Jackson Laboratory, Bar Harbor, Maine; cat. 004746). Mice from both strains were born with Mendelian frequencies. To induce Nogo-A/B deficiency in endothelial cells, male and female NogoA/B$^{f/f}$-VE-Cad-CreERT2-positive and NogoA/B$^{f/f}$-VE-Cad-CreERT2-negative littermates were injected intraperitoneally (i.p.) with 6 mg/kg of tamoxifen daily for 5 d at the age of 6–8 weeks. The extent of Cre-mediated excision of exon 2 and 3 of *Rtn4* in endothelial cells and VSMCs was confirmed by real-time PCR on endothelial cells isolated from mouse lungs and on endothelial cell and VSMC mRNA isolated from the thoracic aorta of NogoA/B$^{f/f}$, EC-NogoA/B-deficient and SMC-NogoA/B-deficient mice. All animal experiments were approved by the Weill Cornell Institutional Animal Care and Use Committee. The experiments were not randomized; investigators were blinded for blood pressure measurements by tail-cuff system but not for allocation during experiments and outcome assessment.

Blood pressure measurements in conscious mice. Systolic, diastolic and mean blood pressure was measured in conscious 12-week-old male mice using the pneumatic tail-cuff method (MRBP System, Life Science, Woodland Hills, California). Briefly, animals were placed in a plastic chamber maintained at 34 °C and a cuff with a pneumatic pulse sensor was attached to the tail. After 1 week of training, three consecutive measurements were performed per mouse, and the values were averaged. In another set of experiments, mice were injected with myriocin (0.3 mg/kg i.p., Sigma) or vehicle (0.4% fatty acid–free BSA) and blood pressure was measured 1 d later.

Evaluation of vascular reactivity in pressure myograph. Carotid and second-order mesenteric arteries isolated from male mice at 10–12 weeks of age were carefully cleaned from adhering tissue and mounted on glass micropipettes in a pressure myograph chamber (Danish MyoTechnology, Aarhus, Denmark); the orientation of the vessel in relation to the flow *in vivo* was maintained. Viability of the vessels was maintained using Krebs solution (in mM: NaCl 118, KCl 4.7, $MgCl_2$ 1.2, KH_2PO_4 1.2, $CaCl_2$ 2.5, $NaHCO_3$ 25 and glucose 10.1), at 37 °C and oxygenated (95% O_2 and 5% CO_2).

The micropipette was connected to a pressure interface, which regulated intraluminal pressure and flow. The vessel diameter was monitored in real time using a microscope connected to a digital video camera (IC Capture) and computer software with edge detection capability. Mesenteric arteries were equilibrated for 30 min at 80 mm Hg, preconstricted with PE (1 μM) and a cumulative concentration-response curve of Ach (1×10^{-9}–3×10^{-5} M) was performed to evaluate the integrity and the function of the endothelium. Normotensive vessels with less than 80% vasodilatory response to Ach were discarded.

To evaluate the vasoconstriction of mesenteric arteries, cumulative concentration-response curves were performed with PE (1×10^{-9}–3×10^{-5} M, Sigma), U-46619 (1×10^{-12}–10^{-6} M, Sigma) and S1P (1×10^{-9}–10^{-6} M, Avanti Polar Lipids); to assess the vasodilation of mesenteric arteries, cumulative concentration curves were performed with Ach (1×10^{-9}–3×10^{-5} M) and S1P (1×10^{-12}–3×10^{-9} M). The cumulative concentration-response curve for Ach was performed in the presence of L-NAME (NOS inhibitor; 100 μM, Sigma), indomethacin (COX inhibitor; 10 μM, Sigma) and a combination of both, added in Krebs buffer (mM: NaCl 118, KCl 4.7, $MgCl_2$ 1.2, KH_2PO_4 1.2, $CaCl_2$ 2.5, $NaHCO_3$ 25 and glucose 10.1).

The myogenic response was measured using a stepwise increase of intraluminal pressure (20, 45, 70, 95, 120 mm Hg); each pressure level was maintained for 5 min. At the end of the experiment, a myogenic curve was performed in Ca^{2+}-free Krebs buffer supplemented with 1 mM EGTA. Myogenic tone (%) was expressed as $[(D_1 - D_2)/D_1] \times 100$, where D_1 is the passive diameter in Ca^{2+}-free Krebs buffer and D_2 is the active diameter in complete Krebs buffer, at the same intraluminal pressure.

Flow-mediated vasodilation was measured using preconstriction of mesenteric arteries with PE (3×10^{-7} M) at 95 mm Hg of mean pressure. Intraluminal flow was increased in steps of 25 μl/min from 0 to 125 μl/min. Flow was maintained for 5 min at each step. Measurements of myogenic tone and flow-mediated vasodilation were repeated after 45 min of incubation of mesenteric arteries with 1 μM or 100 nM W146 (Sigma), a selective and reversible $S1P_1$ inhibitor. Carotid arteries were assessed for vasoconstriction induced by increasing concentration of PE (1×10^{-9}–3×10^{-5} M). To evaluate the vasodilation induced by flow, carotid arteries were preconstricted with a concentration of PE inducing 60% of the maximum vasoconstriction achieved in the concentration-response curve to PE, followed by a stepwise increase of flow (0 to 800 μl/min).

Vessel morphometry and immunostaining. Following full relaxation with Ach (1×10^{-6} M), mesenteric arteries were fixed with 4% PFA and left overnight at 4 °C. The elastic lamina of paraffin-embedded mesenteric arteries was visualized with Verhoeff's Van Gieson (VVG) staining. Wall thickness, area and radius were determined by using a computerized image-analysis system (Image-Pro).

PFA-fixed mesenteric arteries were paraffin-embedded or OCT-embedded. For immunohistochemistry, following deparaffinization and antigen retrieval, mesenteric artery sections were incubated overnight with antibody against Nogo-B (#AF6034, R&D, 1:100) followed by anti-sheep antibody (#713-065-003, Jackson ImmunoResearch, 1:200). Staining was developed with diaminobenzidene (DAB). Finally, the sections were counterstained with Mayer's hematoxylin solution.

For immunofluorescence, frozen mesenteric artery sections were stained for Nogo-B (1:100, R&D) and biotinylated IB4 (1:100, BD Biosciences) overnight at 4 °C, and were then stained with Cy3-labeled anti-sheep antibody (#A21436, Invitrogen, 1:200) and streptavidin–Alexa 488 (#016-540-084, Jackson ImmunoResearch, 1:200) in PBS for 1 h. Nuclei were stained with DAPI. Confocal immunofluorescence images of the tissues were captured on an Olympus Fluoview confocal microscope.

NOx assay. Male mice of 10–14 weeks of age were anesthetized with ketamine (150 mg/kg) and xylazine (15 mg/kg). Whole blood was collected in EDTA via cardiac puncture. Plasma was obtained by centrifugation at 1,000 × *g* for 15 min at 4 °C and was immediately collected and snap frozen in liquid nitrogen to preserve NO content.

NO levels were measured as nitrite in plasma from WT, Nogo-A/B-deficient, NogoA/B$^{f/f}$, EC-Nogo-A/B-deficient and SMC-Nogo-A/B-deficient mice, with or without AngII infusion, using a modified Griess reaction[58]. Briefly, after precipitation of plasma proteins with $ZnSO_4$ (30% w/v), supernatants were chemically reduced with acid-washed (0.24 M HCl) cadmium powder (Sigma-Aldrich). After centrifugation, samples were measured for nitrite content with Griess reagent (0.1% naphtylethylendiamine dihydrochloride in H_2O and 1% sulfaniamide in 5% concentrated H_3PO_4) and read at a wavelength of 550 nm. All samples were assayed in duplicate and the NO concentration was calculated against an $NaNO_2$ calibration curve (0.31, 0.62, 1.25, 2.5, 5, 10, 20, 40, 80 μM).

cGMP measurements. cGMP levels were measured in WT and Nogo-A/B-deficient aortas isolated from male mice at 10–14 weeks of age. Briefly, the aorta was dissected and cleaned from surrounding fat tissue, cut into rings 2 mm in length, and incubated in Krebs at 37 °C for 30 min. After that, rings were stimulated with the Ca^{2+} ionophore A23187 (10 μM, Sigma) for 3 min and were then rapidly weighed and snap frozen in liquid nitrogen. Tissues were homogenized with 20 volumes of 5% trichloroacetic acid (TCA) per gram of tissue and centrifuged at 1,500 × *g* for 10 min. The supernatant was collected and treated with 5 volumes of water-saturated diethylic ether (repeated twice) to extract residual TCA. The samples were warmed for 5 min at 70 °C to remove any residual ether. The cGMP content of the samples was measured by enzyme immunoassay, using a kit according to the manufacturer's instructions (Cayman, CA).

© 2015 Nature America, Inc. All rights reserved.

doi:10.1038/nm.3934

***En face* aorta immunostaining.** Aortas were isolated from male mice at 10–14 weeks of age and immunostaining for eNOS, phosphorylated eNOS and $S1P_1$ receptor was performed as previously described[17].

SMC isolation from mouse aorta. Aortic SMCs were isolated from aortas of 5 WT and 5 Nogo-A/B-deficient male mice at 6–8 weeks of age. Briefly, aortas were cleaned of connective tissue and the adventitia was digested with type II collagenase (Worthington 1 mg/ml) dissolved in DMEM (20 min, 37 °C), followed by its manual removal. Aortas were minced and digested in 0.1 mg/ml elastases (Sigma) and 1 mg/ml collagenase II in DMEM (2 h, 37 °C). VSMCs were cultured in DMEM containing 10% FBS. When cells reached confluence, the medium was replaced with 10% charcoal-stripped DMEM for 24 h. Cell lysates were collected in lysis buffer as previously described[56] and were analyzed for sphingolipid content by the Lipidomic Core Facility of the Medical University of South Carolina.

Endothelial cell isolation from mouse lung tissue. Primary endothelial cells from the lungs (MLECs) of female and male WT, Nogo-A/B-deficient, Nogo-$A/B^{f/f}$ and EC-Nogo-A/B-deficient mice at 6–10 weeks of age were isolated as previously described[56]. The culture medium was replaced with EBM-2 medium supplemented with growth factors (#J64516) and 10% charcoal-stripped FBS for 24 h and cell lysates were collected in lysis buffer as previously described[56]. Cell lysates were analyzed for sphingolipid content by the Lipidomic Core Facility of the Medical University of South Carolina. MLECs isolated from Nogo-$A/B^{f/f}$ and EC-Nogo-A/B-deficient mice were collected, cell lysate was collected in RIPA buffer, and western blotting was performed for Nogo-B protein.

Lentivirus construction. Murine HA-tagged Nogo-B (NCBI AAM77069) was synthesized by Genewiz and inserted in the lentiviral vector pCDH-CMV-MCS-EF1-Puro (Addgene). Lentiviral particles containing the construct encoding HA-tagged Nogo-B were produced in HEK293T cells transfected with Oligofectamine 2000 (Invitrogen). Viral particles were harvested from the culture supernatant 72h after transfection, passed through a 0.45-μm filter and concentrated by adding PEG-*it* virus precipitation solution (#LV810A-1, System Biosciences) overnight at 4 °C followed by centrifugation at 1,500 × *g* for 30 min. Viral pellets were resuspended in DMEM (#D6429, Sigma) and stored at −80 °C until use.

Cell culture and transfection. HEK293T cells were cultured in DMEM (#D6429, Sigma) with high glucose (4,500 mg/L) supplemented with 10% FBS, penicillin and streptomycin (pen/strep, Sigma). Cells were maintained at 37 °C and 5% CO_2 in a humidified incubator. Transfections were as follows: 0.4×10^6 cells were transfected with 2 μg HA-tagged Nogo-B plasmid and 2 μg of SPTLC1 plasmid (#MMM1013-202805259, MGC Mouse Sptlc1 cDNA, GE Healthcare-Dharmacon) using Lipofectamine 2000 (#11668-019, Invitrogen) following the manufacturer's protocols. Cells were harvested 48 h after transfection and coimmunoprecipitation of Nogo-B and SPTLC1 was assessed.

Monkey kidney COS7 cells were cultured in DMEM (Sigma) with high glucose (4,500 mg/L) supplemented with 10% FBS and penicillin and streptomycin (pen/strep, Sigma). Cells were maintained at 37 °C and 5% CO_2 in a humidified incubator. Transfections were as follows: 0.4×10^6 cells were transfected with 2 μg HA-tagged Nogo-B plasmid and 2 μg of SPTLC1 plasmid using Lipofectamine 2000 following the manufacturer's protocols. 48 h after transfection, cells were fixed with 4% PFA and stained for anti-HA (1:100, #11815016001, Roche) and SPTLC1 (1:100, #611304; BD Biosciences) antibodies overnight at 4 °C, and were then stained with Alexa Fluor 594–labeled anti-rat antibody (#A21209, Invitrogen) and streptavidin–Alexa 488 (#016-540-084, Jackson ImmunoResearch, 1:200) in PBS for 1 h. Nuclei were stained with DAPI.

NgBR knockdown in HUVECs by siRNA transfection. siRNA targeting the Nogo-B receptor (NgBR; forward: GGAAAUACAUAGACCUACA, reverse: UGUAGGUCUAUGUAUUUCC) and control (forward: UUCUCCGAACG UGUCACG, reverse: ACGUGACACGUUCGGAGAA) were synthesized by Qiagen. HUVECs were transfected with siRNA using Oligofectamine transfection reagent (Invitrogen). Expression of NgBR (analyzed by western blotting) and the enzymatic activity of SPT were assessed 72 h after transfection.

Measurement of S1P in medium. Confluent WT and Nogo-A/B-deficient MLECs were incubated with DMEM containing 10% charcoal-stripped FBS, 10 mmol/L sodium glycerophosphate, 5 mmol/L sodium fluoride and 1 mmol/L semicarbazide[12] for 4 h. In another set of experiments, MLECs were treated with myriocin (100 nM) dissolved in 0.1% fatty acid–free BSA or vehicle. After 20 h, 10 mmol/L sodium glycerophosphate, 5 mmol/L sodium fluoride and 1 mmol/L semicarbazide[5] were added to the MLECs, and 4 h later the culture medium was collected and analyzed for S1P content by the Lipidomic Core Facility of the Medical University of South Carolina.

Sphingolipid analysis by LC-MS/MS. Plasma, medium, endothelial cell and VSMC lysates were used for quantification of sphingolipids by LC-MS/MS. The levels of ceramide (Cer) species, sphingosine (Sph) and S1P were analyzed by the Lipidomics Analytical Core at the Medical University of South Carolina as previously described[59].

Western blot and immunoprecipitation. Western blot and immunoprecipitation analyses were performed as previously described[56]. For western blot analysis, the following primary antibodies were used: Nogo-B (#AF-6034; R&D, Minneapolis, MN, dilution 1:1,000); eNOS, SPTLC1 and Hsp90 (#610297, #611304 and #610419; BD, Biosciences, San Jose, CA; dilution 1:1,000); nNOS and phospho-S^{1176}-eNOS (#C12H1 and #9571s respectively; Cell Signaling Technology, Danvers, MA; dilution 1:1,000); anti-HA (#11867423001; Roche, Nutley, NJ; dilution 1;1,000); $S1P_1$, c-Myc, ORMDL1/2/3, VE-cadherin and NgBR (#sc-25489, 1:2,000; #sc-40, 1:1,000; #sc-161143, #sc-6458, 1:1,000; and #sc138044 1:1,000, respectively; Santa Cruz Biotechnology, Santa Cruz, CA); Calnexin (#ADI-SPA-860-D; ENZO, Farmingdale, NY; dilution 1:1,000); α-SMA and β-actin (#5228 and #A2228; Sigma Aldrich, St. Louis, MO; dilution 1:2,000); anti-GFP (#ab6556; abcam, Cambridge, MA; dilution 1:1,000). For immunoprecipitation analysis, the following antibodies were used: Nogo-B (#AB-163; Kinasource, Scotland, UK; dilution 1:100) and anti-HA (#11815016001; Roche; dilution 1:100).

Microsomal isolation from mouse lung. Microsomal fractions were obtained from WT and Nogo-A/B-deficient lungs as previously described[60]. Briefly, a volume of 50 mM HEPES buffer (pH 7.4 at 4 °C), 0.25 M sucrose, and 5 mM EDTA (pH adjusted to 7.4 with NaOH) was added to the lung (equal to the lung weight, 1 g/ml). Additional buffer was added to yield a 20% (w/v) suspension and the lung was homogenized with three 15-s treatments with a Brinkman Polytron PT20. The homogenates were centrifuged for 15 min at 18,000 × *g* at 4 °C, and the resulting supernatants were centrifuged for 1 h at 100,000 × *g*. The microsomal pellets were then resuspended by adding 1 ml of buffer (50 mM HEPES (pH 7.4 at 25 °C), 5 mM EDTA (pH 7.4), 5 mM DTT and 20% (w/v) glycerol) per gram of lung tissue used for the microsome preparation.

Serine palmitoyltransferase (SPT) activity. SPT activity in lung tissue was measured as previously described[60]. Briefly, the assay was conducted in a volume of 0.1 ml that contained: 0.1 M HEPES (pH 8.3 at 25 °C), 5 mM DTT, 2.5 mM EDTA (pH 7.4), 50 μM pyridoxal 5′-phosphate (PLP; Sigma), 0.45 μM [^{3}H]serine (PerkinElmer), 0.2 mM palmitoyl-CoA (Sigma) and 50 μg microsomes. The control reaction contained all of the above components except palmitoyl-CoA. The samples were incubated for 10 min at 37 °C and the reaction was stopped with 0.2 ml of 0.5 N NH_4OH, followed by 50 μl of $NaBH_4$ (5 mg/ml) to convert the reaction product 3-ketosphinganine into sphinganine. Radiolabeled lipid products were extracted by using a modification of Bligh and Dyer's method[61]. Briefly, 0.7 ml $CHCl_3$ and methanol (1:2) was added, followed by $CHCl_3$ and 0.5 N NH_4OH (1:1). After centrifugation, the lower layer containing lipids was collected and the organic solvent was removed under a gentle stream of nitrogen gas. The samples were dissolved in $CHCl_3$ and analyzed by thin-layer chromatography.

For measurement of SPT activity in HUVECs and MLECs isolated from WT and Nogo-A/B-deficient mice, the cells were grown to confluence in 60-mm dishes and starved in endothelial growth basal medium (EBM2) medium for 3 h. After washing twice with PBS, the cells were suspended in SPT reaction buffer (1 M HEPES (pH 8.3 at 25 °C), 5 mM DTT, 2.5 mM EDTA (pH 7.4) and 50 μM pyridoxal 5′-phosphate) and sonicated for 15 s. Cell lysates (200 μg) were mixed

© 2015 Nature America, Inc. All rights reserved.

with 0.45 μM [^{3}H]serine and 0.2 mM palmitoyl-CoA. As a negative control, an aliquot of cell lysate was treated with myriocin (100 nM) for 6 h. The reaction was carried out for 10 min at 37 °C and stopped by the addition of NaBH (5 mg/ml) for 5 min at room temperature. The radiolabeled lipid products were extracted using the modified Bligh and Dyer's method, as described above.

Thin-layer chromatography analysis. Separation and quantification of lipids was performed by thin layer chromatography (TLC silica gel 60, Merck). Sphinganine, sphingomyelin, ceramide and phosphatidylserine (Avanti Polar Lipids) were used as standards. TLC plates were developed with chloroform/methanol/ammonium hydroxide (65:25:4). [^{3}H]serine-labeled sphinganine was quantified using a TLC scanner (radioactivity TLC analyzer RITA, Raytest Straubenhardt, Germany); amounts of radiolabeled lipid were determined using a [^{3}H]serine calibration curve.

RNA extraction from aortic endothelial cells and VSMC and real-time PCR analysis. Endothelial cells and VSMCs were isolated from aortas of NogoA/B$^{f/f}$, EC-Nogo-A/B-deficient and SMC-Nogo-A/B-deficient mice. Briefly, the aorta was dissected and quickly cleaned from surrounding fat tissue. The aorta was cannulated and perfused with 400 μl TRIzol for 10 s to isolate endothelial cells. The perfusate was collected in a tube and the aorta was snap frozen in liquid nitrogen and homogenized in 400 μl TRIzol to isolate VSMCs. Total RNA from perfusate and tissue was extracted according to the TRIzol reagent protocol (Thermo Scientific). Reverse transcription was then performed using 100 ng of RNA and Maxima Reverse Transcriptase (200 U/μl) supplied with 5× buffer (250 mM Tris-HCl (pH 8.3 at 25 °C), 375 mM KCl, 15 mM MgCl2, 50 mM DTT; Thermo Scientific, USA). The real-time PCR analysis was done with an iCycler Applied Biosystems 7700, using SYBR green PCR Master Mix (Qiagen, USA). Nogo-B primers were used to evaluate the efficiency of Nogo-B knockdown in endothelial cells and VSMCs from EC-Nogo-A/B-deficient and SMC-Nogo-A/B-deficient mice. VE-cadherin and αSMA primers were used to evaluate the purity of the isolated cells. Nogo-B, VE-cadherin and αSMA mRNA levels were normalized using the housekeeping gene *GAPDH*. The following primers were used for REAL-TIME PCR: Nogo, forward (GGTGCCTTGTTCAATGGTTT) and reverse (ATTCTGCTTTGCGCTTCAAT); VE-cadherin, forward (TAG CAAGAGTGCGCTGGAGATTCA) and reverse (ACACATCATAGCTGG TGGTGTCCA); αSMA, forward (CAGGGAGTAATGGTTGGAAT) and reverse (TCTCAAACATAATCTGGGTCA); GAPDH, forward (AGGTCGGTG TGAACGGATTTG) and reverse (TGTAGACCATGTAGTTGAGGTCA).

Assessment of Nogo-B expression in aortas from SMC-Nogo-A/B-deficient mice. Aortas from Nogo-A/B$^{f/f}$ and SMC-Nogo-A/B-deficient mice were isolated and cleaned from surrounding connective tissue. Endothelial cells from the aorta were mechanically removed with a cannula followed by perfusion with 1 ml of distilled water to wash out any residual endothelial cells. The adventitia was digested with type II collagenase (Worthington 1 mg/ml) dissolved in DMEM (20 min, 37 °C), followed by its manual removal. Aortas were washed in PBS and snap frozen in liquid nitrogen and homogenized in RIPA buffer to perform western blot analysis.

Chronic infusion of AngII. AngII (500 ng/kg/min) was infused using an osmotic minipump (model ALZET 2004) (ref. 62). Briefly, minipumps were implanted subcutaneously in WT, Nogo-A/B-deficient, NogoA/B$^{f/f}$, EC-Nogo-A/B-deficient and SMC-Nogo-A/B-deficient male mice at 10 weeks of age. Blood pressure was monitored twice per week from day 0 to day 28 of AngII infusion. Vascular reactivity was evaluated as described above. In another set of experiments, WT and Nogo-A/B-deficient mice received myriocin (My; 0.3 mg/kg i.p.) at day 25, and blood pressure was measured at days 26, 27 and 28. In another set of experiments, WT and Nogo-A/B-deficient mice were injected with SEW2187 ($S1P_1$ agonist, 3 mg/kg i.p., Cayman) or vehicle (DMSO), and blood pressure was measured at different time points.

Statistical analysis. Data are expressed as mean ± s.e.m. One-way or two-way ANOVA with *post hoc* Bonferroni's test was run for all statistical analyses except where a Student's *t*-test analysis was used. Differences were considered statistically significant when $P < 0.05$. All tests were two-sided. GraphPad Prism software (version 5.0, GraphPad Software, San Diego, CA) was used for all statistical analysis. The s.d. considered for the calculation was estimated on the basis of previous published studies using the tail-cuff system to measure blood pressure in mice and by preliminary experiments of vascular reactivity using mesenteric arteries from three mice.

57. Wang, Y. *et al.* Ephrin-B2 controls VEGF-induced angiogenesis and lymphangiogenesis. *Nature* **465**, 483–486 (2010).
58. Bryan, N.S. & Grisham, M.B. Methods to detect nitric oxide and its metabolites in biological samples. *Free Radic. Biol. Med.* **43**, 645–657 (2007).
59. Bielawski, J. *et al.* Sphingolipid analysis by high performance liquid chromatography-tandem mass spectrometry (HPLC-MS/MS). *Adv. Exp. Med. Biol.* **688**, 46–59 (2010).
60. Williams, R.D., Wang, E. & Merrill, A.H. Jr. Enzymology of long-chain base synthesis by liver: characterization of serine palmitoyltransferase in rat liver microsomes. *Arch. Biochem. Biophys.* **228**, 282–291 (1984).
61. Bligh, E.G. & Dyer, W.J. A rapid method of total lipid extraction and purification. *Can. J. Biochem. Physiol.* **37**, 911–917 (1959).
62. Cao, X. *et al.* Angiotensin II-dependent hypertension requires cyclooxygenase 1-derived prostaglandin E2 and EP1 receptor signaling in the subfornical organ of the brain. *Hypertension* **59**, 869–876 (2012).

© 2015 Nature America, Inc. All rights reserved.

doi:10.1038/nm.3934